

Influence of invasive quagga mussels, phosphorus loads, and climate on spatial and temporal patterns of productivity in Lake Michigan: A biophysical modeling study

Mark D. Rowe ^{1*}, Eric J. Anderson,² Henry A. Vanderploeg,² Steven A. Pothoven,³ Ashley K. Elgin,³ Jia Wang,² Foad Yousef⁴

¹University of Michigan, Cooperative Institute for Limnology and Ecosystems Research, Ann Arbor, Michigan

²National Oceanic and Atmospheric Administration, Great Lakes Environmental Research Laboratory, Ann Arbor, Michigan

³National Oceanic and Atmospheric Administration, Great Lakes Environmental Research Laboratory, Muskegon, Michigan

⁴Department of Civil and Environmental Engineering, University of California Los Angeles, Los Angeles, California

Abstract

We applied a three-dimensional biophysical model to Lake Michigan for the years 2000, 2005, and 2010 to consider the mechanisms controlling spatial and temporal patterns of phytoplankton abundance (chlorophyll *a*) and lake-wide productivity. Model skill was assessed by comparison to satellite-derived Chl *a* and field-measured water quality variables. We evaluated model sensitivity to scenarios of varying mussel filter feeding intensity, tributary phosphorus loads, and warm vs. cool winter-spring climate scenarios. During the winter-spring phytoplankton bloom, spatial patterns of Chl *a* were controlled by variables that influenced surface mixed layer depth: deep mixing reduced net phytoplankton growth through light limitation and by exposing the full water column to mussel filter feeding. Onset of summer and winter stratification promoted higher surface Chl *a* initially by increasing mean light exposure and by separating the euphotic zone from mussels. During the summer stratified period, areas of relatively high Chl *a* were associated with coastal plumes influenced by tributary-derived nutrients and coastal upwelling-downwelling. While mussels influenced spatial and temporal distribution of Chl *a*, lake-wide, annual mean primary production was more sensitive to phosphorus and warm/cool meteorology scenarios than to mussel filter feeding scenarios. Although Chl *a* and primary production declined over the quagga mussel invasion, our results suggest that increased nutrient loads would increase lake-wide productivity even in the presence of mussels; however, altered spatial and temporal patterns of productivity caused by mussel filter feeding would likely persist.

The invasive dreissenid mussels, *Dreissena polymorpha* (zebra mussel) and *D. rostriformis bugensis* (quagga mussel) continue to spread in North America and Europe, altering ecology and biogeochemistry of invaded lakes (Brown and Stepien 2010; Karatayev et al. 2014), and raising questions regarding how lake management strategies should respond. Since 2000, Lake Michigan has experienced rapid growth of the quagga mussel population (Nalepa et al. 2009; Rowe et al. 2015b), declining pelagic primary production (Fahnenstiel et al. 2010), and increased nuisance benthic algae production (Auer et al. 2010; Brooks et al. 2014). Declining productivity and prey fish abundance (Bunnell et al. 2014)

have raised concern over sustainability of economically and culturally important fisheries.

It is not obvious whether declines in chlorophyll *a* and primary production after the quagga mussel invasion can be attributed to the direct effect of filter feeding on phytoplankton abundance, or to declining total phosphorus (TP). Several studies have implicated quagga mussel filter feeding on phytoplankton as a direct cause of declining productivity. Fahnenstiel et al. (2010) showed that reduced productivity occurred in times of deep mixing when benthic filter feeders could remove phytoplankton from the full water column. Vanderploeg et al. (2010) showed that quagga mussel clearance rates are sufficient to exceed phytoplankton growth rates under the assumption of a well-mixed water column and Rowe et al. (2015a) showed the same result under realistic vertical mixing conditions representative of the spring isothermal period. Other studies implicated declining phosphorus concentration in addition to the direct effects of

*Correspondence: mark.rowe@noaa.gov

Additional Supporting Information may be found in the online version of this article.

filter feeding. Pothoven and Fahnenstiel (2013) showed reduced productivity not only during periods of deep mixing, but also during the summer stratified period. Other investigations showed statistical association between reduced TP and reduced productivity (Bunnell et al. 2014; Warner and Lesht 2015). Spring TP concentration has declined over the time period of the quagga mussel invasion, thus statistical analyses have limited ability to discern the independent effects of correlated variables: filter feeding vs. declining phosphorus. Mechanistic models are complementary to statistical analyses, having the ability to test mechanistic hypotheses under constraints of mass conservation and realistic rates for biological processes and transport.

Phosphorus loading targets are the primary management variable that could be adjusted to influence productivity in Lake Michigan, which is considered to be a phosphorus-limited system (Chapra and Sonzogni 1979). A phosphorus loading target of 5600 metric tons (10^3 kg) per annum (MTA) was set in the 1978 Great Lakes Water Quality Agreement. The target load has not been exceeded since 1981 (Chapra and Dolan 2012). Phosphorus loads and in-lake concentration declined from 1980 to 2008 due to a ban of phosphorus in detergents, and reduced phosphorus in treated wastewater (Dolan and Chapra 2012). Over the more recent period 1994–2008, there was no significant trend in TP load ($p = 0.93$, H_0 of zero slope), and the mean load was 3500 MTA with 20% relative standard deviation indicating substantial inter-annual variation (data: Dolan and Chapra 2012, their Table 8).

Reduced primary production offshore combined with increased benthic productivity nearshore create a management paradox for initiatives to revisit phosphorus loading targets under the revised GLWQA of 2012 (Great Lakes Water Quality Protocol 2012); increased phosphorus loads may benefit fisheries production, but may exacerbate nuisance benthic algae production nearshore, while further reduction in lake-wide productivity could undermine fisheries production, risking a crash of the economically-valuable salmon fishery. In Lake Huron, biomass of alewives, the preferred prey of stocked Pacific salmon, collapsed between 2002 and 2003, resulting in declining recreational harvests of salmon. Statistical analysis did not identify a clear cause of the crash (Bunnell et al. 2014), while food web and fisheries models suggested a combination of top-down and bottom-up causes (He et al. 2014; Kao et al. 2016).

The spatial distribution of resources is of increasing interest in post-dreissenid Lake Michigan. Increased water clarity and reduced productivity offshore have altered food web interactions between phytoplankton, zooplankton, and prey fish (Vanderploeg et al. 2015). Nearshore energy subsidies provide increased support to fishes and invertebrates (Turschak et al. 2014). Because of the differing management requirements of nearshore and offshore productivity, it is increasingly necessary to develop an understanding of the

factors controlling the spatial distribution of phytoplankton, zooplankton, and productivity in dreissenid-invaded lakes, including the influence of tributary nutrient loads, meteorology, and in-lake transport (Bootsma et al. 2015).

We applied a three-dimensional biophysical model to Lake Michigan to investigate the independent effects of dreissenid mussel filter feeding, tributary nutrient loads, and meteorology on spatial and temporal patterns of productivity in Lake Michigan. Calibration and skill assessment was conducted for the years of the lake-wide benthic surveys (2000, 2005, and 2010), which spanned the quagga mussel invasion. We conducted a series of model sensitivity simulations with varied levels of dreissenid mussel filter feeding intensity, nutrient loads, and cool vs. warm winter-spring meteorological scenarios expected to be representative of changing climate conditions. We evaluated the response of several variables related to productivity to the model scenarios, including Chl *a* concentration, phosphorus concentration, zooplankton abundance, quagga mussel growth, and lake-wide mean primary production.

Methods

Observational data

Observational data from several sources were used for model skill assessment. Physical and water quality data were obtained from United States Environmental Protection Agency (USEPA) and National Oceanic and Atmospheric Administration (NOAA) field studies. NOAA buoys 45002 and 45007 in north and south Lake Michigan, respectively, provided water surface temperature (www.ndbc.noaa.gov/, accessed January 2013). The NOAA Episodic Events—Great Lakes Experiment (EEGLE) study (1998–2000) provided ship-based Chl *a*, TP, and dissolved phosphorus (DP) measurements (<https://www.glerl.noaa.gov/res/projects/eegle/data/data.html>, accessed January 2013). Additional vertically-resolved temperature, Chl *a*, TP, and DP data were obtained from annual US EPA spring and summer surveys, and the Lake Michigan Mass Balance study (1994–1995) (www.epa.gov/greatlakes/monitoring/data_proj, accessed April 2012). Vertically-resolved temperature, Chl *a*, TP, DP, and particulate organic carbon (POC) concentrations were measured at long-term ecological research stations located in a nearshore-offshore transect from Muskegon at 110-m, 45-m, and 15-m bathymetric depth, M110, M45, and M15, respectively (Fig. 1), detailed methods are reported elsewhere (Fahnenstiel et al. 2010; Pothoven and Fahnenstiel 2013). Zooplankton biomass at the Muskegon transect were from Vanderploeg et al. (2012) Pothoven and Fahnenstiel (2015) and Pothoven (unpubl.).

A plankton survey system (PSS; Vanderploeg et al. 2009) was used to map continuous profiles of temperature and Chl *a* along the Muskegon transect from the 10-m to the 110-m depth contour (Fig. 1). The PSS was raised and lowered at ~ 0.25 m s^{-1} in a sinusoidal path from 1 m to 2 m beneath

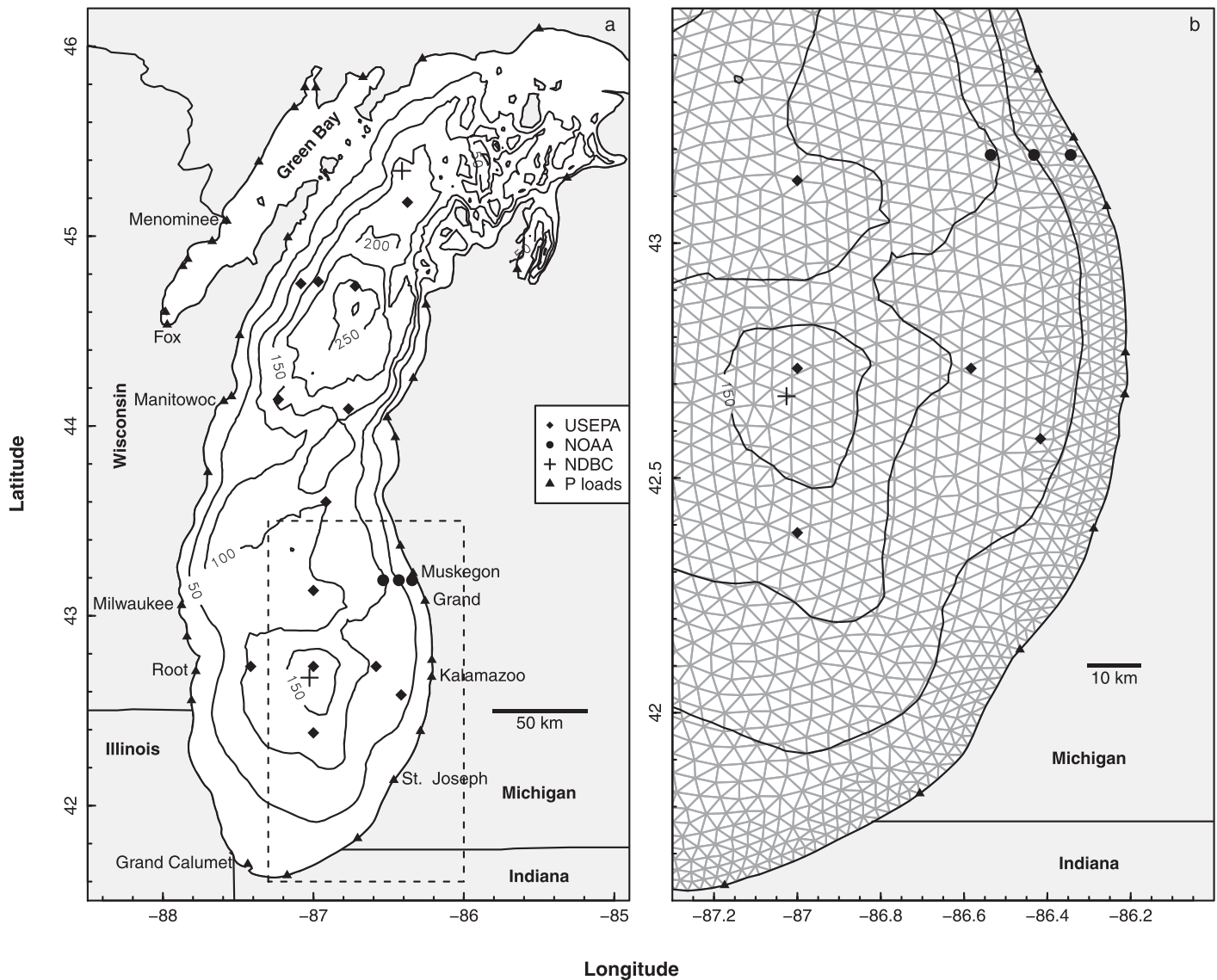


Fig. 1. Map of Lake Michigan, showing bordering U.S. states of Michigan, Indiana, Illinois, and Wisconsin. **(a)** Spatial domain of the hydrodynamic model (white area), bathymetry (50-m contours), and locations of U.S. Environmental Protection Agency stations (USEPA), National Oceanic and Atmospheric Administration stations offshore of Muskegon (NOAA), National Data Buoy Center buoys (NDBC), and locations of tributary phosphorus loads (P loads). Names are indicated for the ten highest-loading tributaries. **(b)** Enlarged area of southeastern Lake Michigan, showing a portion of the unstructured hydrodynamic model grid and station locations.

the surface to 2–4 m above the bottom as the R/V *Laurentian* moved at $\sim 1.8 \text{ m s}^{-1}$ (Vanderploeg et al. 2009). The PSS recorded data every 0.5 s from multiple sensors mounted on a V-fin, including a Chl *a* fluorometer (Wet Labs ECO Fluorometer, Sea-Bird Scientific) and a conductivity-temperature-dissolved-oxygen sensor (Sea-Bird 19 plus V2). Plots of PSS variables and model data used linear interpolation (R package “akima,” Akima 1978). Fluorometer output (volts) was converted to derived Chl *a* concentration by regression of fluorometer output on laboratory Chl *a* measurements of field samples matched to PSS location and time ($r^2 = 0.81$, $n = 59$).

Satellite-derived data included temperature, Chl *a*, and light penetration. Water surface temperature was obtained from NOAA Coast Watch Great Lakes Surface Environmental Analysis (GLSEA) (<https://oceancolor.gsfc.nasa.gov/>, accessed January 2013). Chl *a* and K_{d490} were obtained from SeaWiFS (Sea-viewing Wide Field-of-view Sensor) daily L2 data (<http://oceancolor.gsfc.nasa.gov>, accessed June 2014) using OC4 algorithm (Yousef et al. 2014). We estimated K_{dPAR} from SeaWiFS K_{d490} using the empirical relationship of Saulquin et al. (2013), as used by Fahnenstiel et al. (2016).

Phosphorus in mussel tissue

Quagga mussels were collected at 45-m and 25-m stations offshore of Muskegon on a total of eight dates in 2008, 2013, and 2014, and stored frozen. Mussels were analyzed as composite samples of 5–20 individuals. After measuring shell length, soft tissue was removed, dried at 65–70°C overnight, weighed, and ground with a pestle in tared weighing pans. Tissue was combusted at 500°C for 2 h in glass tubes, then oxidized to orthophosphate with 25 mL of 1N HCl in a hot water bath (95–99°C) for 60 min (Andersen 1976). After dilution to 0.019 N HCl, phosphorus was analyzed using the ascorbic acid method (Johengen et al. 2013) on a QuAAatro[®], Continuous Segmented Flow Analyzer System (Seal Analytical, Mequon, Wisconsin).

Hydrodynamic model

We applied the finite volume community ocean model (FVCOM) to Lake Michigan (Rowe et al. 2015a). FVCOM (v. 3.1.6) is an unstructured grid, finite-volume, free surface, three-dimensional primitive equation ocean model that solves the momentum, continuity, temperature, salinity (set to zero here), and density equations (Chen et al. 2003). Turbulence closure was implemented through the MY-2.5 scheme for vertical mixing (Galperin et al. 1988), and the Smagorinsky scheme for horizontal mixing. External and internal time steps were 10 s. The unstructured grid consisted of 5795 nodes and 10,678 elements, with 20 terrain-following vertical (sigma) layers of uniform thickness, with mean element side lengths of 2.6 km near the coast (< 30-m depth), and 4.0 km elsewhere, with greater resolution (~ 1 km) in areas of complex coastline morphology (e.g., where Green Bay meets the main lake). The lateral boundaries were closed; bi-directional flow at the Straits of Mackinac and a minor outflow through the Chicago diversion were not simulated (Fig. 1). Ice cover was not simulated. Annual maximum ice cover in Lake Michigan (25% average) typically occurs in mid-February (Wang et al. 2012; Supporting Information Fig. S1).

Atmospheric forcing data were generated by interpolation of hourly observations from 18 stations surrounding Lake Michigan, with empirical adjustment for modification of land-based meteorology over the lake using computer codes developed for use in the NOAA Great Lakes Coastal Forecasting System (Schwab and Beletsky 1998; Beletsky et al. 2003). When available, wind speed, direction, and air temperature were used in the interpolation from NOAA buoys 45002 and 45007 (Fig. 1). Atmospheric forcing variables were eastward and northward components of 10-m wind velocity, air temperature, relative humidity, downward shortwave, and downward longwave radiation. Upward longwave radiation was calculated in FVCOM using the simulated water surface temperature. Surface fluxes of momentum, sensible heat, and latent heat were calculated by the NOAA COARE bulk algorithm (v. 2.6) (Fairall et al. 1996). The model was

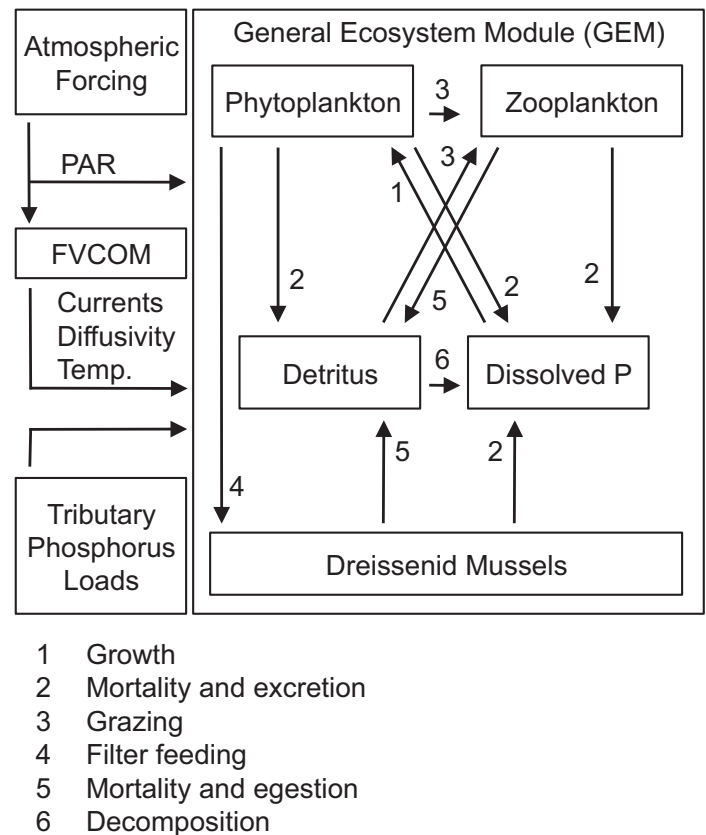


Fig. 2. Process diagram showing biological model compartments, process pathways, and transfer of external forcing data.

initialized on 01 January 2000, 01 January 2005, or 01 January 2010, using satellite-derived surface temperature (see Observational data), and setting salinity and current velocities set to zero.

Biological model

The biological model consisted of a conventional four-compartment nutrient-phytoplankton-zooplankton-detritus (NPZD) model with the addition of a fifth compartment to represent benthic filter feeder (dreissenid mussel) biomass. The NPZD model was implemented using the FVCOM general ecosystem module (GEM), which allows the user to specify biological model compartments within a flexible framework, and solves the three-dimensional scalar advection-diffusion equations on the FVCOM unstructured grid. FVCOM-GEM has been applied previously to study spatially-resolved plankton dynamics in coastal marine systems (Tian and Chen 2006; Ji et al. 2008a,b) and in Lake Michigan (Luo et al. 2012) using NPZD and NPZ models. We added the dreissenid mussel compartment to the FVCOM-GEM code (described below).

The five compartments of the biological model represented DP (limiting nutrient), detritus (nonliving organic particles), phytoplankton, zooplankton, and mussel biomass (Fig. 2). A fixed phosphorus : carbon ratio of 0.016 by mass

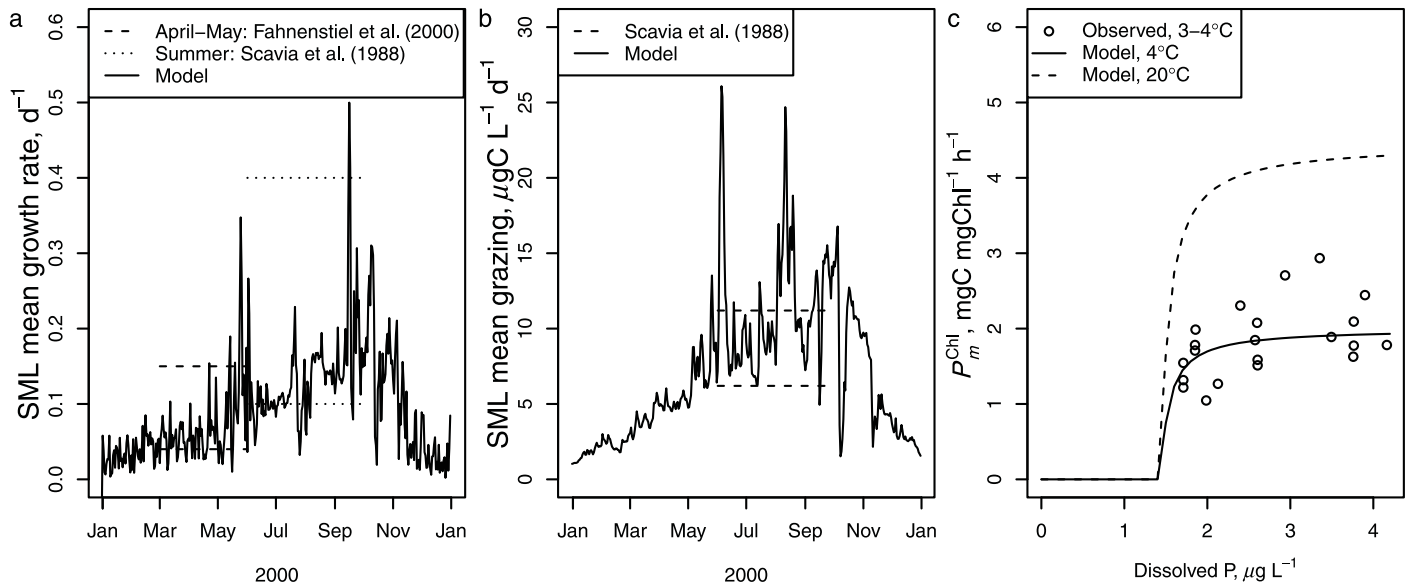


Fig. 3. Comparison of key process rates to observations. The solid line in (a) and (b) are from model output at the 110-m station offshore of Muskegon (Fig. 1). (a) SML mean phytoplankton growth rate and comparable literature values. (b) SML mean zooplankton grazing rate. (c) Dependence of P_m^{Chl} on DP concentration for the model parameterization (lines) and values from Lohrenz et al. (2004) re-plotted on a DP scale for guidance (see Methods).

was assigned to mussel biomass, plankton biomass, and detritus, which is within the measured range of Lake Michigan seston, (0.007–0.042, Pothoven and Fahnenstiel 2013), and mussel tissue (see Results and Discussion). Nutrient uptake by phytoplankton was represented using Michaelis-Menten kinetics. Zooplankton were allowed to graze on phytoplankton, detritus, and zooplankton using the generalized Michaelis-Menten functional response with exponent $m=2$ (Tian 2006; Ji et al. 2008a). A quadratic predation closure term was applied to zooplankton (Steele and Henderson 1992). The phytoplankton production-irradiance curve was formulated as by Fahnenstiel et al. (1989, 2016), as described by Rowe et al. (2015a) with the Chl a : carbon ratio fixed at 0.036 (0.026–0.04, Fahnenstiel et al. 1989). Phytoplankton and detritus were assigned settling velocities of 0.2 m d^{-1} (phytoplankton 0.1 – 0.35 m d^{-1} , Fahnenstiel and Scavia 1987; detritus 0.14 – 0.4 m d^{-1} , Dayton et al. 2014).

Photosynthetically-active radiation (PAR) incident at the surface was calculated from hourly incident short-wave irradiance values used to force FVCOM: 1 W m^{-2} short-wave irradiance $\approx 1.678 \mu\text{E m}^{-2} \text{ s}^{-1}$ PAR (Fahnenstiel et al. 2016). Sub-surface PAR in GEM is calculated using an attenuation coefficient parameterized as a linear function of particulate model state variables,

$$K_{\text{dPAR}} = a_w + a_p P_{\text{Chl}} + a_d D \quad (1)$$

where P_{Chl} is the phytoplankton Chl a concentration, D is the detritus concentration, a_w, a_p, a_d are empirical coefficients that were calibrated within literature values to give K_{dPAR} values comparable to observations, and to simulate the

increase in water clarity that was observed after the quagga mussel invasion; $a_w = 0.07 \text{ m}^{-1}$, $a_p = 0.03 \text{ mgChl}^{-1} \text{ m}^2$ (0.02–0.03), $a_d = 0.2 \text{ g-detritus-C}^{-1} \text{ m}^2$ (0.08–0.25, assuming 0.46 gC/gVSS) (Di Toro 1978; Lohrenz et al. 2004).

The biological model was calibrated for 2000, prior to major effects of the quagga mussel invasion (Vanderploeg et al. 2010; Rowe et al. 2015b), then simulations were run for 2005 and 2010 using the same set of parameter values. Key process rates were confirmed to be within the range of literature values for Lake Michigan (Scavia et al. 1988; Fahnenstiel et al. 2000), including phytoplankton growth and zooplankton grazing (Fig. 3a,b). Threshold and half-saturation parameters for uptake of DP by phytoplankton (Fig. 3c) were set using measurements of photosynthetic rate vs. soluble reactive phosphorus (SRP) by Lohrenz et al. (2004). A linear regression of DP vs. SRP using data from the Lake Michigan Mass Balance study (see Observational data) was used to relate SRP measured by Lohrenz et al. (2004) to the model state variable (DP), and to establish the nutrient threshold ($1.4 \mu\text{g L}^{-1}$), representing the pool of DP that was assumed to be biologically unavailable.

A benthic filter feeder bioenergetic model was added to GEM (after Schneider 1992; Cerco and Noel 2010), and parameterized to represent Lake Michigan quagga mussels. The rate of change of mussel biomass was calculated as,

$$\frac{dM}{dt} = (f_a F_A P - r_b) M \quad (2)$$

where M is mussel biomass, f_a is the fraction assimilated, F_A is the biomass-specific filtration rate, P is the phytoplankton

biomass concentration in the bottom model layer, and r_b is the base respiration rate. High and low estimates of the temperature-dependent filtration rate were taken from Vanderploeg et al. (2010), using the linear regressions of F_A vs. temperature (1–7°C) in their Fig. 2 for feeding on a desirable food (*Cryptomonas*) and on Lake Michigan seston, respectively. Filtration rates measured over the range 7–25°C did not show significant temperature dependence (Vanderploeg unpubl.), so F_A was limited to ≤ 25 mL mg-ash-free-dry-tissue-mass⁻¹ h⁻¹, the maximum value reported by Vanderploeg et al. (2010). Mussel biomass carbon was estimated from ash-free-dry-tissue-mass (AFDM) as 1 g dry-tissue-mass = 0.88 g AFDM, 1 g dry-tissue-mass = 0.46 g carbon (Nalepa et al. 1993). It was assumed that 30% of filtered food particles were egested as detritus (Schneider 1992), 30% was the energetic cost of feeding (Schneider 1992) (phosphorus fraction was excreted as DP), and the remainder went to increase mussel biomass. The base respiration rate (0.006 d⁻¹), respiration temperature dependence, and the maximum assimilation rate (4% of mussel biomass per day) were set following the assumptions and literature citations of Bocaniov et al. (2014). Mortality and predation were neglected.

Tributary phosphorus loads

Dolan and Chapra (2011, 2012) estimated annual tributary dissolved and TP loads to Lake Michigan for the period 1994–2008 at 38 tributary locations (Fig. 1). We distributed annual loads to a daily mass flux value using the daily fraction of annual discharge (assumption of constant concentration) from the nearest stream flow gage (<http://waterdata.usgs.gov/>, accessed September 2014). Loads were added to the model cell adjacent to the tributary location; DP was added to the DP model variable, and particulate phosphorus (TP minus DP) was added to the detritus variable, after conversion to carbon equivalent. In addition, an atmospheric phosphorus load of 310 MTA (10³ kg yr⁻¹) (Dolan and Chapra 2012) was applied uniformly in space and time. For the 2010 simulation, annual phosphorus loads averaged over the most recent years available after 2005 (2006–2008) were used, distributed to daily fluxes using 2010 discharge data. The TP load to Lake Michigan in the 2000, 2005, and 2010 simulations was 3100 MTA, 2800 MTA, and 3300 MTA.

Skill statistics

Agreement between modeled and observed data was quantified using the Pearson correlation coefficient (r), bias deviation (BD) and root mean square deviation (RMSD),

$$BD = \frac{1}{n} \sum_{i=1}^n (S_i - O_i) \quad (3)$$

$$RMSD = \left[\frac{1}{n} \sum_{i=1}^n (S_i - O_i)^2 \right]^{1/2} \quad (4)$$

where S_i , O_i are the simulated and observed values at a given location and time, and n is the number of observations.

Model sensitivity scenarios

We conducted model simulations to represent actual conditions over the course of the quagga mussel invasion for 2000, 2005, and 2010 (“baseline” simulations). Additional sensitivity scenarios were conducted to show the influence of quagga mussels, tributary phosphorus loads, and meteorological conditions (Table 1). Model simulations were initialized on 01 January of each year and run for 12 months without data assimilation. Phytoplankton biomass was initialized to produce simulated Chl *a* consistent with January–February satellite-derived values in each year (1.0 $\mu\text{g L}^{-1}$ Chl *a*, 0.5 $\mu\text{g L}^{-1}$ Chl *a*, and 0.25 $\mu\text{g L}^{-1}$ Chl *a* in 2000, 2005, and 2010, respectively). Zooplankton biomass was initialized at 5–7 $\mu\text{g C L}^{-1}$ (Vanderploeg et al. 2012, their Fig. 4a). DP was initialized in the main lake (excluding Green Bay, see Fig. 1) as a spatially-uniform value based on a volume-weighted mean of the USEPA spring survey field samples for the corresponding year. The detritus variable was initialized so that the TP (summed over all NPZD) matched the volume weighted mean value from the USEPA spring survey. Green Bay dissolved and TP were initialized using field samples from the Lake Michigan Mass Balance study (1994–1995); additional effort would be required to accurately simulate water quality in eutrophic Green Bay, but this was not the focus of our study. The mussel biomass spatial distribution was initialized in simulations for 2000, 2005, and 2010 using the mussel distribution maps of Rowe et al. (2015b) obtained from application of a geostatistical model to lake-wide surveys of mussel densities by Ponar grab sample (Nalepa et al. 2009). The filter feeding intensity, or fraction of the water column cleared per day under vertically well-mixed conditions, calculated from the initial mussel spatial distributions and clearance rate scenarios, is shown in Fig. 4. Finally, a high phosphorus scenario was simulated in which the 2010 phosphorus load was scaled up by a factor of 1.7 to match the target load of 5600 MTA established in the Great Lakes Water Quality Agreement (Dolan and Chapra 2012).

Results

Model skill assessment

The model simulated major spatial and temporal patterns in observed temperature and water quality variables. A brief description of model skill assessment is provided here with full detail given in Supporting Information. The model simulated surface temperature with reasonable skill (absolute BD < 0.46°C, RMSD < 1.41°C, Supporting Information Fig. S2, Supporting Information Table S1) in comparison to buoy and satellite-derived observations. In addition, the oscillating thermocline position caused by upwelling-downwelling dynamics at the Muskegon 45-m station was simulated (BD < 0.8°C, RMSD < 2.1°C, Supporting Information Fig. S3). In 2000, seasonal patterns of monthly mean satellite-derived Chl *a* (BD = 0.05 $\mu\text{g L}^{-1}$, RMSD = 0.24 $\mu\text{g L}^{-1}$, $r = 0.57$) and

Table 1. Model scenarios. Mussel biomass spatial distribution was initialized from Rowe et al. (2015b) for the given year, or not simulated (-). DP and TP (summed over all model variables) were initialized from a volume-weighted average of the USEPA GLNPO spring survey data for the year(s) indicated. Phosphorus load was set from Dolan and Chapra (2012), or at the target load of 5600 MTA. Meteorology was from the year being simulated, except for cool and warm spring scenarios in which case meteorology was from 1997 or 1998, respectively. The quagga mussel clearance rate was set at high or low values based on feeding experiments by Vanderploeg et al. (2010) on *Cryptomonas* or Lake Michigan seston, respectively.

Description	Initial mussels	Initial TP, DP	TP, DP load	Meteorology	Clearance rate
Mussels, loads*	2000	2000	2000	2000	Seston
Mussels, loads*	2005	2005	2005	2005	Seston
Mussels, loads*	2010	2010	2010	2010	Seston
No mussels, loads	-	2000	2000	2000	Seston
No mussels, loads	-	2005	2005	2005	Seston
No mussels, loads	-	2010	2010	2010	Seston
Mussels, no loads	2000	2000	None	2000	Seston
Mussels, no loads	2005	2005	None	2005	Seston
Mussels, no loads	2010	2010	None	2010	Seston
High clearance	2010	2010	2010	2010	<i>Cryptomonas</i>
Mussels, loads, cool	2010	2010	2010	1997	Seston
High clearance, cool	2010	2010	2010	1997	<i>Cryptomonas</i>
No mussels, loads, cool	-	2010	2010	1997	Seston
No mussels, loads, warm	-	2010	2010	1998	Seston
Mussels, loads, warm	2010	2010	2010	1998	Seston
High clearance, warm	2010	2010	2010	1998	<i>Cryptomonas</i>
No mussels, high P	-	1983–1989	5600 MTA	2010	Seston
Mussels, high P	2010	1983–1989	5600 MTA	2010	Seston
High clearance, high P	2010	1983–1989	5600 MTA	2010	<i>Cryptomonas</i>

* “Baseline” scenarios, used for model calibration and skill assessment.

K_{dPAR} ($\text{BD} = -0.01 \text{ m}^{-1}$, $\text{RMSD} = 0.02 \text{ m}^{-1}$, $r = 0.48$), were simulated showing maxima in spring and fall with a minimum in mid-summer (Fig. 5a,d). Reduced Chl *a* and light attenuation in 2005 and 2010, compared to 2000, were simulated (Fig. 5b,c,e,f). At the Muskegon transect in 2000, the model simulated major patterns in Chl *a* concentration, including surface maxima in spring and fall, a deep Chl *a* layer during summer stratification, and higher Chl *a* concentrations nearshore (15-m station) than offshore (Fig. 6, abs. $\text{BD} < 0.4 \mu\text{g L}^{-1}$, $\text{RMSD} < 1.0 \mu\text{g L}^{-1}$, $r > 0.52$). Reduced Chl *a* concentration during deep mixing periods was simulated in 2005 and 2010, relative to 2000, although April–May Chl *a* was biased high in the model (Fig. 6c,f,i). Simulated POC, dissolved and TP fell generally within the range of observations (relative bias -3% to 15% USEPA, -50% to 18% NOAA), although correlation was less than for Chl *a* concentrations. Zooplankton biomass in 2000 was within the range of observations at Sta. M110, although the seasonal maximum in mid-summer was under-predicted by the model (Supporting Information Fig. S4a). Reduced summer zooplankton biomass was simulated in 2010 vs. 2000, consistent with observations (Supporting Information Fig. S4c).

The model simulated major features of the spatial distribution of Chl *a* in Lake Michigan, in comparison to satellite-

derived and field observations (Supporting Information Fig. S5). A circular pattern of low Chl *a* in the center of southern Lake Michigan surrounded by higher Chl *a* in mid-depth regions, which has been referred to as the “doughnut”-shaped phytoplankton bloom (Kerfoot et al. 2008), was observed and simulated in March and April prior to the quagga mussel invasion, but not in 2005 or 2010 post-invasion. During the summer stratified period in July and August, low surface Chl *a* concentration was observed and simulated offshore, with plumes of higher Chl *a* concentration extending from the shore. Animations of model surface Chl *a*, and model state variables, are included in Supporting Information to illustrate the dynamics of these nearshore Chl *a* plumes, a process that is difficult to visualize by field observations or through infrequent cloud-free satellite images. Surface Chl *a* concentration increased from September to October or November (Fig. 6; Supporting Information Fig. S5g–i) and became more uniform, consistent with observations.

Modeled change in mussel biomass

Simulated mussel growth rates were at a maximum in March–May, and again increased in October–November (Fig. 7), times that were characterized by relatively high Chl *a*

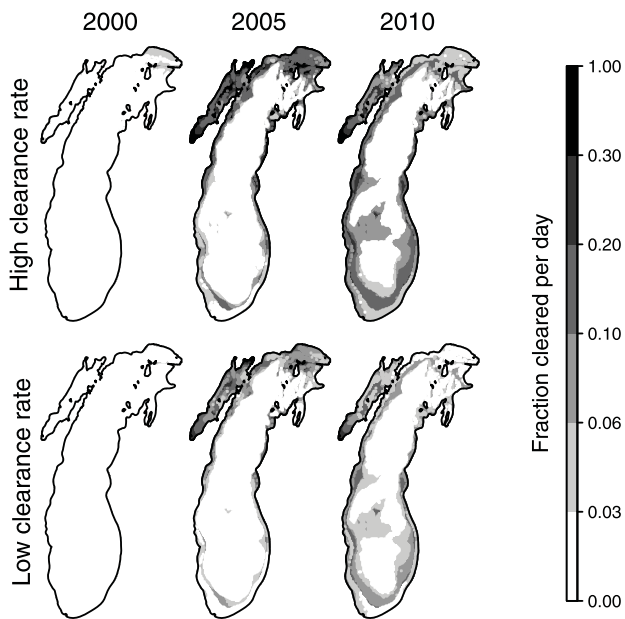


Fig. 4. Fraction of the water column cleared per day under vertically well-mixed conditions (Rowe et al. 2015b) resulting from the initial mussel biomass distributions and clearance rate scenarios used in the model simulations.

concentration and deep mixing. Simulated mussel growth decreased from nearshore to offshore in 2000, associated with the nearshore-offshore gradient in Chl *a*. Net growth over the year was greater in 2000 than in 2005 or 2010 (Fig. 7), associated with increase in mussel biomass and decrease in Chl *a* over the same period. An animation of mussel ration (ratio of food intake to biomass) is included in Supporting Information to illustrate how dynamic changes in surface mixed layer (SML) depth influenced food availability to mussels on the bottom.

The lake-wide inventory of phosphorus contained in mussel soft tissue increased from 2000 to 2010, while particulate phosphorus associated with detritus decreased over the same period. The model was initialized using volume-weighted mean USEPA spring survey TP and DP (mean TP, $4.6 \mu\text{g L}^{-1}$, $3.4 \mu\text{g L}^{-1}$, $3.0 \mu\text{g L}^{-1}$; DP, $2.0 \mu\text{g L}^{-1}$, $1.9 \mu\text{g L}^{-1}$, $1.9 \mu\text{g L}^{-1}$ for 2000, 2005, and 2010, respectively), resulting in relatively little decrease in dissolved, but a stronger decrease in particulate phosphorus from 2000 to 2010 (Fig. 8, detritus). Our model did not attempt to simulate the loss processes of phosphorus from Lake Michigan, which caused TP inventory to increase by 12–16% at the end of each 12-month simulation due to the watershed phosphorus load (Fig. 8, “sum” vs. “sum-loads”); however, this did not influence year-to-year change in phosphorus inventory because each simulation was initialized from observed values. Our measurements of phosphorus in quagga mussel tissue gave a mean phosphorus : carbon mass ratio in tissue of 0.017 (SD 0.001

for nine composite samples, assuming 0.46 gC/gDW), slightly greater than the value of 0.016 that we used in model simulations based on preliminary data. Insufficient data were available to investigate seasonal or interannual variation in tissue phosphorus.

Sensitivity of Chl *a* spatial and seasonal patterns to quagga mussels, nutrient loads, and meteorology

Model scenarios with increased mussel filter feeding had lower surface Chl *a* in periods of deep mixing. In April 2010, the bands of low Chl *a* concentration in mid-depth regions ($\sim 30\text{--}70 \text{ m}$) were not simulated in the “No mussels” sensitivity scenario, causing a return of the southern basin doughnut pattern in April (Fig. 9a vs. b), while the low Chl *a* bands were enhanced in the “High clearance” scenario (Fig. 9a vs. c). As noted earlier, February–April Chl *a* was biased high in the 2010 simulation using the low estimate of clearance rate. The “High clearance” scenario reduced February–April 2010 Chl *a* relative to the low clearance scenario and improved the skill statistics (BD, $-0.01 \mu\text{g L}^{-1}$ vs. $0.03 \mu\text{g L}^{-1}$; RMSE, $0.36 \mu\text{g L}^{-1}$ vs. $0.38 \mu\text{g L}^{-1}$; r , 0.39 vs. 0.34, for high vs. low clearance, respectively). Quagga mussel filter feeding reduced Chl *a* concentration along the Muskegon transect at times when the SML contacted the bottom, and in addition reduced near-bottom Chl *a* during the summer stratified period (Fig. 10a vs. b,d vs. e,g vs. h).

Surface Chl *a* concentration was sensitive to winter stratification, which limited the SML depth. At the Muskegon 110-m station, there was a simulated and observed vertical gradient in Chl *a* concentration in March 2010 associated with winter stratification (Fig. 10g). In a nearshore-offshore transect from Muskegon on 24 March 2010, higher Chl *a* occurred in areas where the surface cooled below 4°C (Fig. 11 a,i), which was also simulated by the model (Fig. 11b,j) although isothermal conditions extended further offshore in the model than observed. On 14 April 2010, isothermal conditions were observed and simulated along the Muskegon transect (Fig. 11k,l). High Chl *a* was observed nearshore, with a gradient to low Chl *a* offshore, consistent with the model simulation (Fig. 11c,d). Mussel filter feeding reduced Chl *a* concentration, relative to the “No mussels” scenario, at mid-depth and offshore locations where isothermal conditions extended to the bottom and mussel filter feeding intensity was high in both March (Fig. 11b vs. f) and April (Fig. 11d vs. h, Fig. 4).

Nearshore Chl *a* concentration was sensitive to tributary phosphorus loads. The “No loads” scenario caused a reduction in nearshore Chl *a* with little effect offshore (Fig. 9a vs. d). Finally, the “High phosphorus” scenario increased Chl *a* lake-wide, even in the presence of quagga mussel filter feeding (Fig. 9a vs. e): April BD relative to SeaWiFS Chl *a* increased from $0.22 \mu\text{g L}^{-1}$ to $0.76 \mu\text{g L}^{-1}$ and annually from $0.03 \mu\text{g L}^{-1}$ to $0.7 \mu\text{g L}^{-1}$ for baseline and “High P” 2010 scenarios, respectively. As an additional example, the “No

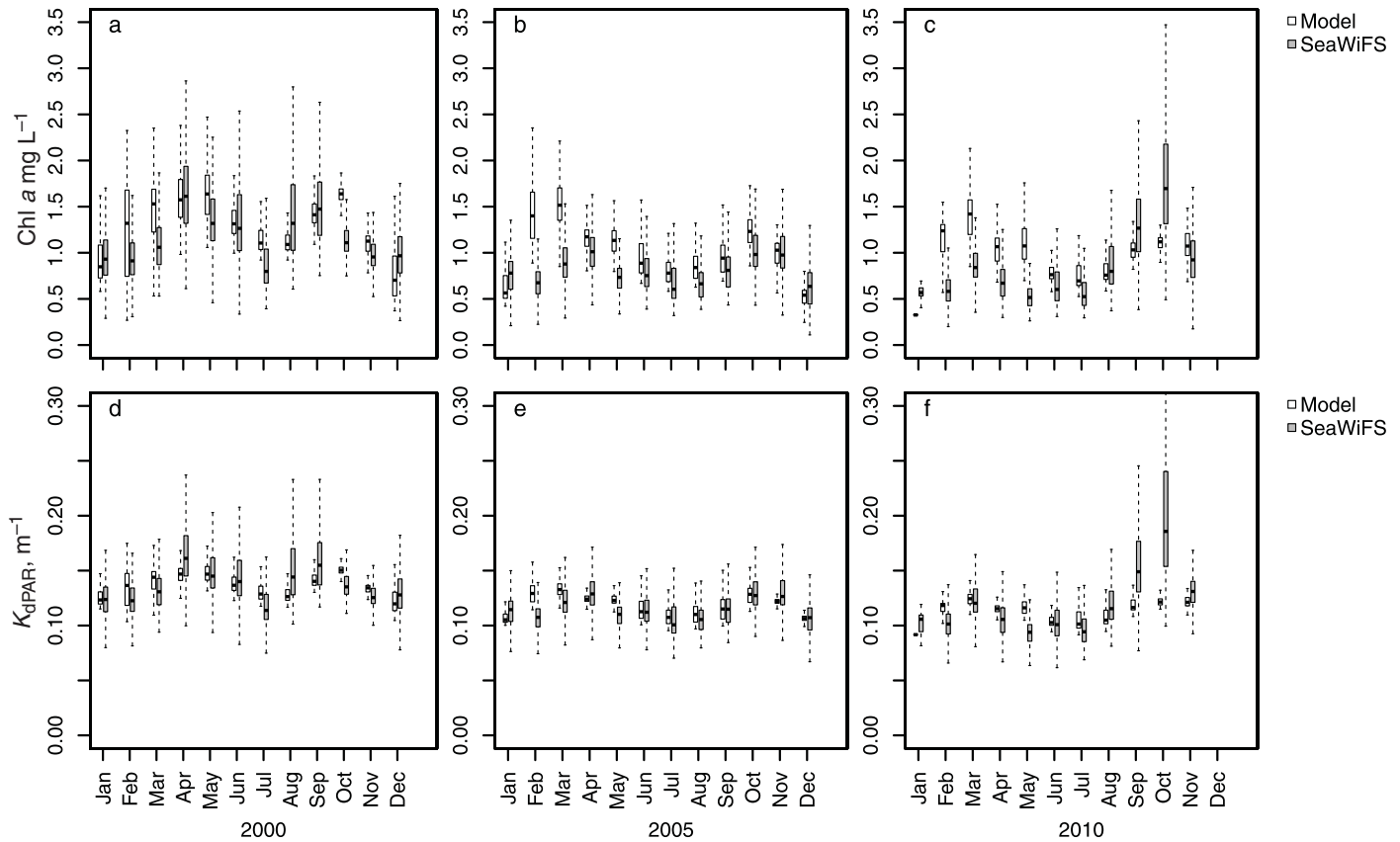


Fig. 5. Modeled and satellite-derived (SeaWiFS OC4) monthly mean surface Chl *a* (a-c) and attenuation coefficient for PAR, K_{dPAR} (d-f), for the 2000, 2005, and 2010 baseline simulations. Boxplots represent spatial variation.

loads” scenario caused low-biased Chl *a* in May–December at the relatively nearshore 15-m and 45-m stations along the Muskegon transect (Fig. 10a vs. c,d vs. f), but minimally affected at the offshore 110-m station (Fig. 10g vs. i).

In the summer stratified period, surface Chl *a* was sensitive to phosphorus scenarios, but not sensitive to mussel filter feeding, as illustrated in Fig. 9 by comparing the baseline scenario (Fig. 9f vs. k) to sensitivity scenarios. In August and September, “No mussels” and “High clearance” scenarios had little effect on surface Chl *a* (Fig. 9f–h,k–m). The “No loads” scenario reduced, but did not eliminate, enhanced Chl *a* along the western shore associated with upwelling (Fig. 9f vs. i,k vs. n). In the “High P” scenario, surface Chl *a* increased while maintaining similar spatial patterns to the baseline scenario. August and September mean Chl *a* increased by $0.8 \mu\text{g L}^{-1}$ and $1.1 \mu\text{g L}^{-1}$ relative to the 2010 baseline scenario.

Sensitivity of surface Chl *a* to mussel filter feeding returned in November, as the deepening SML contacted the bottom. Bands of low-Chl *a* were present in mid-depth areas associated with mussel scenarios (Fig. 9p–s). In the “High P” scenario, mean Chl *a* increased by $0.5 \mu\text{g L}^{-1}$ relative to the 2010 baseline scenario (Fig. 9t), even in the presence of quagga mussels.

Spatial patterns of Chl *a* were sensitive to cool (1997) and warm (1998) winter-spring meteorological scenarios, which modified SML depth. In the “No mussels” scenario, Chl *a* was higher where SML depth was limited by winter stratification and lower in areas of deep mixing (Fig. 12g,h); in the absence of mussels, these patterns were associated with SML depth (Fig. 12j,k). Mussel filter feeding reduced Chl *a* concentration mainly in areas where the SML contacted the bottom (Fig. 12a,b,d,e vs. g,h). In April, winter stratification continued to protect phytoplankton from mussel filter feeding over much of the lake in the cool scenario (Fig. 12b,e vs. h, 1997), but in the warm scenario deep mixing resulted in low Chl *a* in deep basins even in the absence of mussels (Fig. 12g,h, 1998) and reduced Chl *a* in mid-depth locations with mussels (Fig. 12b,e vs. h, 1998). In May, the situation reversed, with deep mixing initiating in the cool scenario (1997 meteorology). The onset of summer stratification in the warm scenario (1998 meteorology) limited SML depth, which was associated with enhanced Chl *a* (Fig. 12c,f vs i).

Sensitivity of lake-wide mean primary production to quagga mussels, nutrient loads, and meteorology

Modeled primary production for the 2000, 2005, and 2010 baseline scenarios was 5.8 Tg C yr^{-1} , 5.3 Tg C yr^{-1} ,

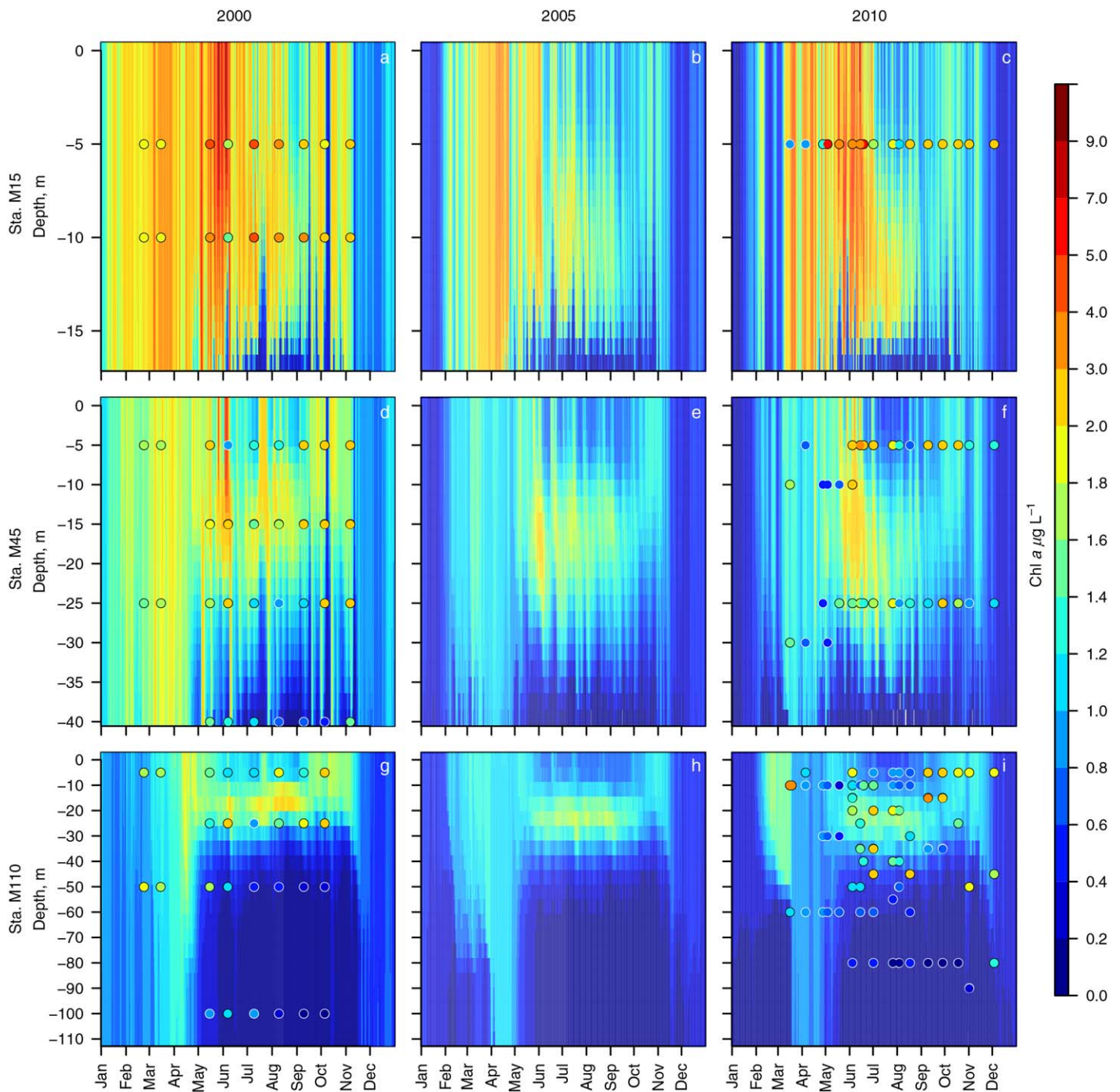


Fig. 6. Time series of vertical distribution of Chl *a* at the 15-m (a-c), 45-m (d-f), and 110-m (g-i) depth NOAA Muskegon transect stations (Fig. 1) for the 2000, 2005, and 2010 baseline simulations. Modeled and field-sampled Chl *a* (symbols) are plotted using the same color scale.

and 5.2 Tg C yr^{-1} , respectively, for the method of Fahnenstiel et al. (2016), compared to $12.9 \text{ Tg C yr}^{-1}$, $12.0 \text{ Tg C yr}^{-1}$, and $12.1 \text{ Tg C yr}^{-1}$, respectively for the method of Warner and Lesht (2015). Using satellite-derived inputs, Fahnenstiel et al. (2016) reported Lake Michigan primary production of $5.0\text{--}6.9 \text{ Tg C yr}^{-1}$ for the years 2010–2013, while Warner and Lesht (2015) reported values of $9.5\text{--}13.6 \text{ Tg C}$

yr^{-1} for the years 1998–2008. The model-derived primary production values were within the range of satellite-derived values reported for the respective methods.

Lake-wide, annual mean primary production was more sensitive to phosphorus and warm/cool meteorology scenarios than to mussel filter feeding scenarios. Simulation of mussel filter feeding reduced primary production by 1–3%,

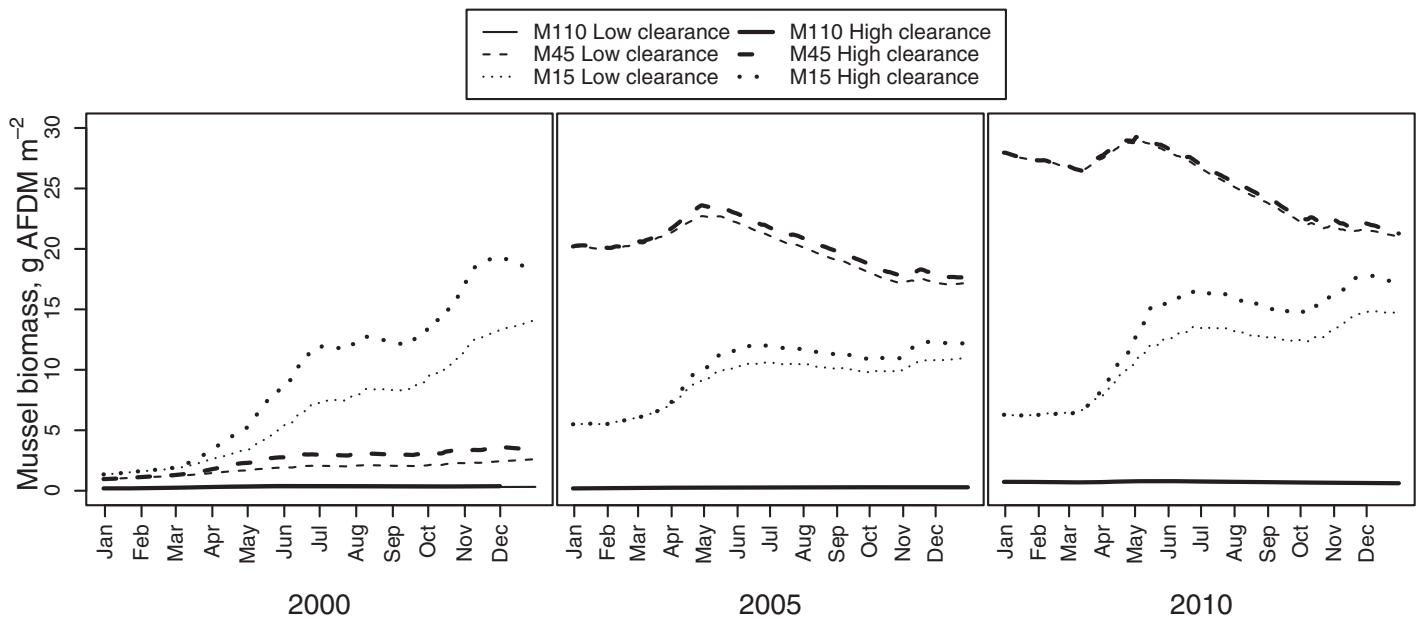


Fig. 7. Modeled quagga mussel biomass at the NOAA stations located at 15-m, 45-m, and 110-m depth offshore of Muskegon for the 2000, 2005, and 2010 baseline simulations, and corresponding sensitivity scenarios with high mussel clearance rate (Table 1).

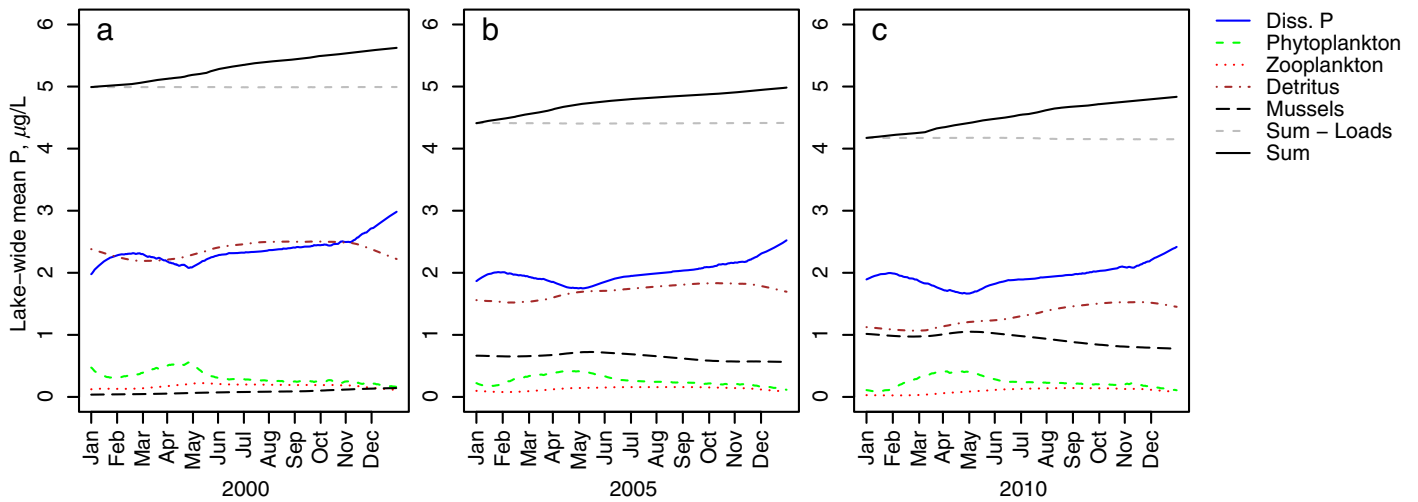


Fig. 8. Components of the lake-wide phosphorus inventory expressed as the mass divided by the lake volume, or the potential contribution of the phosphorus compartment to the lake-wide mean phosphorus concentration for the years 2000 (a), 2005 (b), and 2010 (c).

or 3–6% for the “High clearance” scenario, relative to the “No mussels, Loads” scenario. The 2000 baseline scenario had 7–11% higher primary production (Fig. 13) than the 2010 baseline scenario, representing the combined effect of mussels and lower phosphorus in 2010. The effect of cool (1997) vs. warm (1998) meteorology scenarios was a 9–13% decrease in primary production. Among the “High P” scenarios, all had much higher (24–36%) primary production than the baseline scenario, even with the “High clearance” filter feeding assumption.

Discussion

SML depth influenced spatial patterns of Chl *a*. SML depth along with light attenuation controls mean light exposure to the phytoplankton during the winter–spring transition (Fahnenstiel et al. 2000; Rowe et al. 2015a), as described in the conceptual model of Sverdrup (1953) for initiation of the spring bloom. Kerfoot et al. (2008) attributed formation of the doughnut-shaped winter–spring phytoplankton bloom in southern Lake Michigan to entrainment of nutrients derived from tributaries and

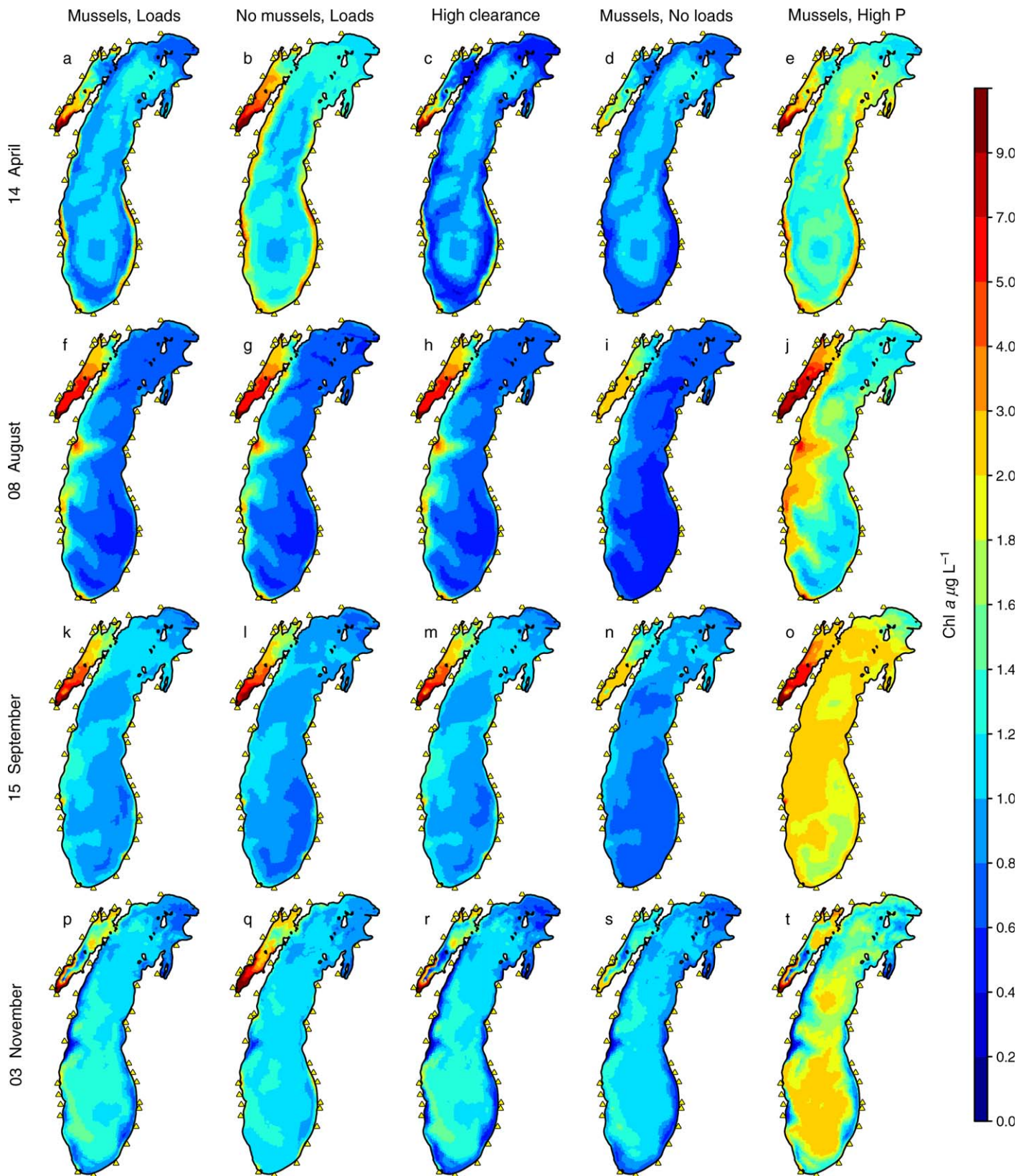


Fig. 9. Model scenarios showing the sensitivity of surface Chl a to quagga mussels and tributary phosphorus loads in seasons characterized by deep mixing (April, **a-e**), summer stratification (August, **f-j**), or deepening of the SML (September/November, **k-t**). Model scenarios were based on the 2010 baseline simulation (**a, f, k, p**) with modifications listed in Table 1.

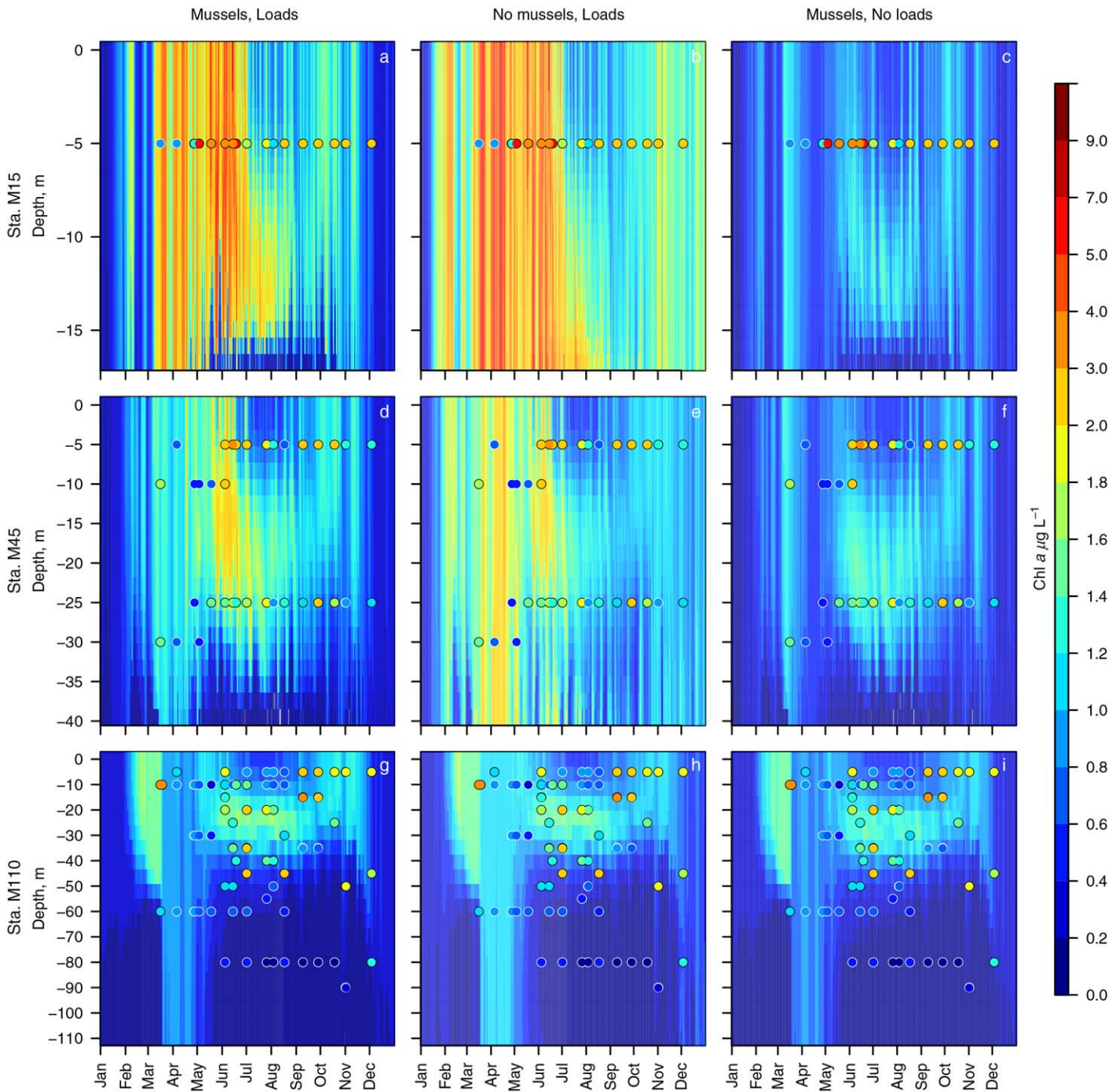


Fig. 10. Sensitivity of Chl *a* concentration to quagga mussels and tributary phosphorus loads at the 15-m (a-c), 45-m (d-f), and 110-m (g-i) depth stations for scenarios based on modification of the 2010 baseline simulation (see Table 1). Modeled and field-sampled Chl *a* (circles) are plotted using the same color scale.

sediment resuspension into the gyre circulation. However, the doughnut pattern was simulated in models that did not include nutrient loads or sediment resuspension, e.g., Fig. 9d and Luo et al. (2012), suggesting that the controlling mechanism is limitation of the SML depth by bathymetry during deep mixing, and associated effect on light exposure averaged over the SML depth. Chl *a* was low in

both the deep southern and northern basins during times of deep mixing (e.g., Fig. 12, April 1998), reflecting the control of SML depth and light limitation by bathymetry in both basins. The maximum density of freshwater occurs at 4°C, thus SML depth can be limited by stratification as a result of cooling below (winter stratification) or warming above (summer stratification) 4°C. Direct observation of

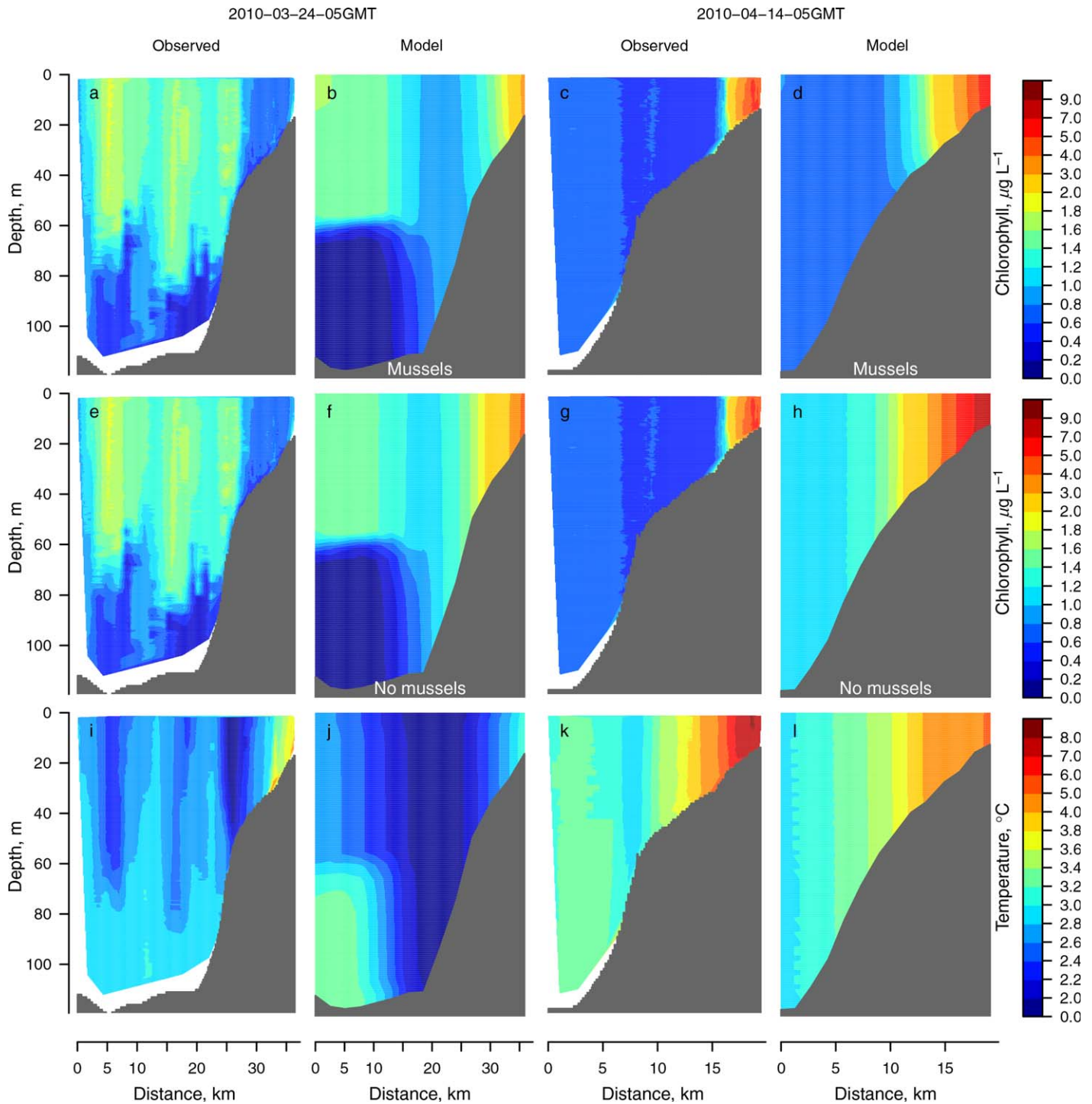


Fig. 11. Comparison of modeled to observed (PSS) Chl *a* concentration (**a-h**) and thermal structure (**i-l**) along the Muskegon transect (Fig. 1) in 2010, showing effects of deep-mixing (April) vs. winter stratification (March, surface cooling < 4°C). Sensitivity of Chl *a* to mussels is shown by comparison of the 2010 baseline simulation (**b,d**) to the corresponding no-mussel scenario (**f,h**). Mussel biomass was maximum at 30–60 m.

enhanced chlorophyll concentration in areas affected by winter stratification was shown in the March 2010 PSS transect (Fig. 11), and winter stratification was shown to influence the March–May spatial patterns of Chl *a* through

the sensitivity of these patterns to meteorological scenarios (Fig. 12).

Quagga mussel filter feeding worked together with light limitation to limit phytoplankton net growth during times

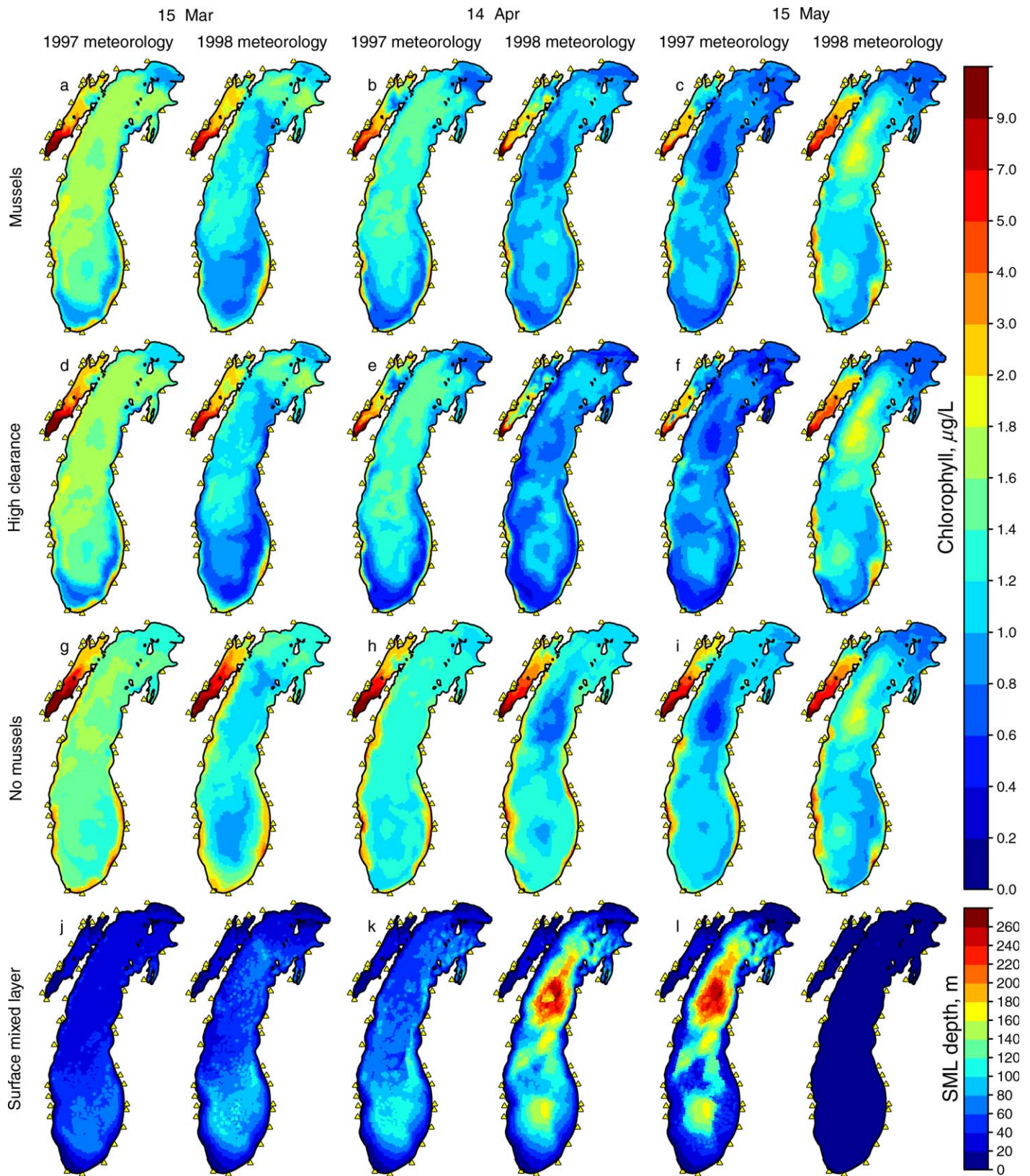


Fig. 12. Model scenarios showing the sensitivity of surface Chl *a* (a-i) and SML depth (j-l) to cool (1997) and warm (1998) winter-spring scenarios in seasons characterized by transition from winter stratification to deep mixing to the onset of summer stratification. Model scenarios were based on the 2010 baseline simulation with substitution of meteorology from 1997 or 1998 (Table 1).

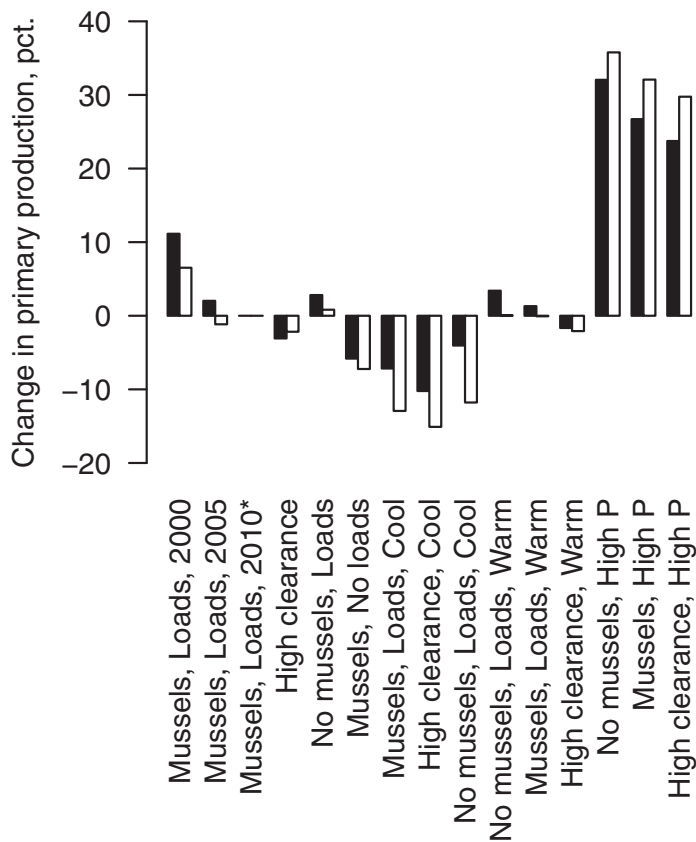


Fig. 13. Change in lake-wide, annual mean primary production (excluding Green Bay) for sensitivity model scenarios (Table 1), relative to the 2010 baseline scenario (*). Primary production was calculated using two methods: filled bar (Fahnenstiel et al. 2016); open bar (Warner and Lesht 2015).

of deep mixing. Reduced Chl *a* occurred in areas of high filter-feeding intensity and deep mixing in model scenarios that included mussels, as observed by Rowe et al. (2015b) who showed a significant association between spatial areas of reduced Chl *a* observed in satellite imagery post-dreissenid invasion and mussel filter feeding intensity that exceeded the benchmark spring phytoplankton growth rate of 0.06 d^{-1} . Rowe et al. (2015a) showed that quagga mussels could reduce Chl *a* during the Lake Michigan spring bloom under realistic estimates of biomass, clearance rate, and vertical mixing in a one-dimensional model simulation. Our three-dimensional model simulations provide a more realistic estimate of the reduction in phytoplankton biomass by filter feeding through inclusion of a realistic spatial distribution of mussel biomass, effects of advection, and by considering sensitivity to low and high estimates of clearance rate. These model results were consistent with previous empirical studies that associated declines in Chl *a* post quagga mussel invasion with seasons of deep mixing (Fahnenstiel et al. 2010; Warner and Lesht 2015).

In the summer stratified period, spatial patterns of Chl *a* were influenced by tributary nutrient loads and coastal upwelling/downwelling with mussel filter feeding having minimal influence. Sensitivity scenarios showed that tributary nutrient loads supported higher Chl *a* nearshore than offshore, in both stratified and unstratified seasons. Lake Michigan nearshore dynamics during summer stratification include internal waves supported by thermal stratification and wind-driven upwelling-downwelling (Troy et al. 2012). Even in scenarios without tributary nutrient loads, upwelling enhanced surface Chl *a* nearshore by bringing the deep Chl *a* layer to the surface, and by enhancing vertical mixing of nutrients and Chl *a* from the hypolimnion into the euphotic zone.

The sensitivity of nearshore Chl *a* to tributary nutrient loads underscores the importance of having accurate estimates of nutrient loads for simulation of Chl *a* and nutrient concentrations nearshore. At the 15-m and 45-m stations of the Muskegon transect, simulated Chl *a* was biased high during the spring isothermal period from mid-March to mid-May (Fig. 10a,d) in the baseline scenario, but better matched observations in the “No loads” scenario (Fig. 10c,f), suggesting that the estimated phosphorus loads may have been too high in this period. The assumption of constant concentration that was used to distribute annual loads to daily values was a coarse approximation; however, limited monitoring data were available.

Simulated mussel growth rates were greater nearshore than offshore and showed seasonal maxima in spring and fall, following spatial and temporal patterns in Chl *a* and mixing depth. These seasonal patterns were consistent with measured quagga mussel condition (ratio of tissue mass to internal shell capacity) at the Muskegon transect; observed condition increased (or decreased least) April through June, decreased June to September, then remained constant or improved slightly in October (Glyshaw et al. 2015). Simulated spatial patterns in mussel growth at the 15-m, 45-m, and 110-m stations were consistent with observed changes in mussel biomass in the comparable $< 30 \text{ m}$, $30\text{--}50 \text{ m}$, and $> 90 \text{ m}$ depth zones by Rowe et al. (2015b). Limited food availability resulted in little simulated mussel growth at the 110-m station (Fig. 7a), consistent with very slow observed increase in biomass over time at depths $> 90 \text{ m}$ (Rowe et al. 2015b). There was a net increase in simulated biomass in 2000 at the 45-m station, but a net decrease in 2005 and 2010 (Fig. 7), showing the effect of food limitation as biomass increased and Chl *a* decreased in the later years. Similarly, observed biomass increased dramatically from 2000 to 2005 in the $30\text{--}50 \text{ m}$ depth range, but increased little from 2005 to 2010 in southern lake Michigan and did not change or declined in central and northern Lake Michigan (Rowe et al. 2015b). Glyshaw et al. (2015) found lower mussel condition at 45 m than at 25 m or 110 m in 2013, suggesting food-limited conditions in the region of peak mussel

biomass, which is consistent with model results. The largest simulated increase in biomass occurred in 2000 at the 15-m station (Fig. 7). Observed biomass increased to 5–10 g AFDM m^{-2} from 2000 to 2005 at depths < 30 m (Rowe et al. 2015b), while simulated biomass increased to 12–18 g AFDM m^{-2} by the end of 2000 (Fig. 7); the model was consistent with observations in showing an increase, although the model over-estimated. The model simulation suggests that food availability for mussels nearshore is high, which is consistent with higher observed mussel condition at the Muskegon 25-m station than at 45 m or 110 m (Glyshaw et al. 2015).

Nearshore mussel biomass may have been overestimated in the model, and may be limited by higher mortality rates, which were not simulated. Small and mid-sized mussels (up to 13 mm) are susceptible to predation by round gobies, *Neogobius melanostomus* (Ghedotti et al. 1995), another Ponto-Caspian invader that is abundant in nearshore Lake Michigan. Predation by gobies has been shown to affect the size structure of mussel populations (Djuricich and Janssen 2001). In addition, mussels may be susceptible to mortality by periodic wave action on sandy substrata that dominate much of Lake Michigan at depths < 30 m (Vanderploeg et al. 2010). In hard substrate areas, such as near Milwaukee, mussels cover ~ 80% of the bottom in waters shallower than 10 m; however, hard substrates cannot be sampled in surveys by Ponar grab sample, so mussel biomass in shallow areas with hard substrate may be underestimated in the maps of Rowe et al. (2015b).

Simulated lake-wide, annual mean primary production declined from 2000 to 2010, consistent with an observed decline in primary production over this period (Fahnenstiel et al. 2010; Warner and Lesht 2015). However, TP concentration and mussel filter feeding intensity both varied over this period, making interpretation of the cause not obvious. Primary production was more sensitive to scenarios of phosphorus and cool/warm meteorology than to scenarios of mussel filter feeding, suggesting that the decline in spring TP over 2000 to 2010 contributed to declining primary production along with the direct effect of filter feeding on phytoplankton biomass, consistent with the finding of Warner and Lesht (2015) from a statistical analysis. The primary production method of Warner and Lesht (2015) produced higher values than the method of Fahnenstiel et al. (2016), as discussed by Fahnenstiel et al. (2016). Because of the differences between the two methods, we chose to present results from both methods in our model sensitivity analysis; however, the two methods showed similar patterns of sensitivity to the model scenarios (Fig. 13).

Relatively low sensitivity of lake-wide, annual mean primary production to mussel filter feeding scenarios may be surprising considering the well-documented disappearance of the spring bloom (Kerfoot et al. 2010; Vanderploeg et al. 2010), reduced Chl *a* (Pothoven and Fahnenstiel 2013; Rowe

et al. 2015a), and reduced primary production (Fahnenstiel et al. 2010) post-mussel invasion. In the absence of reduced TP in the water column, filter feeding alone may shift production spatially and temporally, but during periods of stratification, mussels are separated from the euphotic zone and nutrients that were not taken up earlier during periods of deep mixing may then support phytoplankton production. Relative insensitivity of lake-wide, annual mean primary production to mussel filter feeding may be explained as spatial and temporal redistribution of primary production by mussels, with overall trophic status being determined by the total quantity of limiting nutrient in the water column.

In addition to direct reduction in phytoplankton biomass by filter feeding, mussels may have contributed to the progressive decline in lake-wide phosphorus inventory over the years 2000, 2005, and 2010. In 2010, the lake-wide inventory of phosphorus in mussel soft tissue represented the equivalent of 1 $\mu g L^{-1}$ pelagic phosphorus concentration (Fig. 8c), which can partially, but not fully, account for the decline in pelagic TP of 1.6 $\mu g L^{-1}$ (4.6–3.0 $\mu g L^{-1}$ TP), indicating a net decline in phosphorus inventory even after accounting for the amount transferred to mussel soft tissue. The main process by which phosphorus is lost from Lake Michigan is through sequestration in the sediment (Chapra and Dolan 2012). Chapra and Dolan (2012) applied mass balance models to show that the rate of loss of phosphorus to the sediments increased after the dreissenid invasion for Lakes Michigan, Huron, Erie, and Ontario. Mosley and Bootsma (2015) directly measured the ability of quagga mussels to accelerate the deposition of particulate phosphorus to the sediment in Lake Michigan. Thus, mussels may have contributed to declining primary production by increasing the burial rate of phosphorus into the sediment in addition to sequestering an increasing amount of phosphorus in their soft tissue.

Quagga mussels have had a profound effect on the Lake Michigan ecosystem. Our model simulations showed that quagga mussel filter feeding altered the spatial and temporal distribution of phytoplankton abundance. Our analysis of observational data that was used to develop initial conditions for model simulations showed a progressive decline in lake-wide phosphorus inventory in the water column from 2000 to 2010, which was partially attributed to an increasing inventory of phosphorus in mussel tissue. The redistribution of spatial and temporal patterns of productivity has significant ecological implications. The spring phytoplankton bloom traditionally delivered a fast-sinking pulse of large diatoms to the benthos; this was an important period for copepod egg production (Vanderploeg et al. 1992), and for lipid accumulation in benthic invertebrates including *Mysis diluviana* (Pothoven et al. 2012) and *Diporeia* sp. (Gardner et al. 1990). Phytoplankton size has decreased post-dreissenid invasion (Carrick et al. 2015), likely influencing settling rates and export to the benthos. In addition, the shift to smaller phytoplankton may have negatively affected copepods, the dominant

mesozooplankton consumers, which cannot efficiently feed on phytoplankton $< 3 \mu\text{m}$ (Vanderploeg 1994).

Filter feeding reduces net phytoplankton growth and inhibits nutrient uptake by pelagic production during deep mixing periods, potentially shifting production to other places and times, including stratified periods and nuisance near-shore benthic production. Our sensitivity scenarios showed that even though the quagga mussel invasion coincided with a decrease in lake-wide primary production, increased tributary phosphorus loads would likely increase lake-wide trophic status even in the presence of mussels. However, mussels may mitigate increased productivity over longer time scales than our 1-yr simulations through increased biomass and removal of phosphorus from the water column. Furthermore, increased nutrient loads may exacerbate nuisance benthic algae production. In future management efforts, it will be necessary to consider not only lake-wide productivity, but also the spatial distribution of nutrient sources and their transport to nearshore areas that provide an increasingly important supplement to the pelagic food web, and also support nuisance benthic algae production.

Supporting information

Tables S1–S4, Figures S1–S4, and animation files showing the 12-month “baseline” simulations (Table 1) for 2000, 2005, and 2010; surface temperature, Chl *a*, DP, and detritus; mussel ration, and mussel biomass. Animations may be viewed at <https://deepblue.lib.umich.edu/handle/2027.42/136202>.

References

- Akima, H. 1978. A method of bivariate interpolation and smooth surface fitting for irregularly distributed data points. *ACM Trans. Math. Softw.* **4**: 148–164. doi:10.1145/355780.355786
- Andersen, J. M. 1976. An ignition method for determination of total phosphorus in lake sediments. *Water Res.* **10**: 329–331. doi:10.1016/0043-1354(76)90175-5
- Auer, M., L. Tomlinson, S. Higgins, S. Malkin, E. Howell, and H. Bootsma. 2010. Great Lakes *Cladophora* in the 21st century: Same algae-different ecosystem. *J. Great Lake Res.* **36**: 248–255. doi:10.1016/j.jglr.2010.03.001
- Beletsky, D., D. Schwab, P. Roebber, M. McCormick, G. Miller, and J. Saylor. 2003. Modeling wind-driven circulation during the March 1998 sediment resuspension event in Lake Michigan. *J. Geophys. Res. Oceans* **108**: 3038. doi:10.1029/2001JC001159
- Bocaniov, S. A., R. E. Smith, C. M. Spillman, M. R. Hipsey, and L. F. Leon. 2014. The nearshore shunt and the decline of the phytoplankton spring bloom in the Laurentian Great Lakes: Insights from a three-dimensional lake model. *Hydrobiologia* **731**: 151–172. doi:10.1007/s10750-013-1642-2
- Bootsma, H. A., M. D. Rowe, C. N. Brooks, and H. A. Vanderploeg. 2015. Commentary: The need for model development related to *Cladophora* and nutrient management in Lake Michigan. *J. Great Lake Res.* **41**: 7–15. doi:10.1016/j.jglr.2015.03.023
- Brooks, C., A. Grimm, R. Shuchman, M. Sayers, and N. Jessee. 2014. A satellite-based multi-temporal assessment of the extent of nuisance *Cladophora* and related submerged aquatic vegetation for the Laurentian Great Lakes. *Remote Sens. Environ.* **157**: 58–71. doi:10.1016/j.rse.2014.04.032
- Brown, J. E., and C. A. Stepien. 2010. Population genetic history of the dreissenid mussel invasions: Expansion patterns across North America. *Biol. Invasions* **12**: 3687–3710. doi:10.1007/s10530-010-9763-2
- Bunnell, D. B., and others. 2014. Changing ecosystem dynamics in the Laurentian Great Lakes: Bottom-up and top-down regulation. *BioScience* **64**: 26–39. doi:10.1093/biosci/bit001
- Carrick, H. J., E. Butts, D. Daniels, M. Fehringer, C. Frazier, G. L. Fahnenstiel, S. Pothoven, and H. A. Vanderploeg. 2015. Variation in the abundance of pico, nano, and microplankton in Lake Michigan: Historic and basin-wide comparisons. *J. Great Lake Res.* **41**: 66–74. doi:10.1016/j.jglr.2015.09.009
- Cerco, C. F., and M. R. Noel. 2010. Monitoring, modeling, and management impacts of bivalve filter feeders in the oligohaline and tidal fresh regions of the Chesapeake Bay system. *Ecol. Model.* **221**: 1054–1064. doi:10.1016/j.ecolmodel.2009.07.024
- Chapra, S. C., and W. C. Sonzogni. 1979. Great Lakes total phosphorus budget for the mid 1970s. *J. Water Pollut. Control Fed.* **51**: 2524–2533.
- Chapra, S. C., and D. M. Dolan. 2012. Great Lakes total phosphorus revisited: 2. Mass balance modeling. *J. Great Lakes Res.* **38**: 741–754. doi:10.1016/j.jglr.2012.10.002
- Chen, C., H. Liu, and R. C. Beardsley. 2003. An unstructured grid, finite-volume, three-dimensional, primitive equations ocean model: Application to coastal ocean and estuaries. *J. Atmos. Oceanic Technol.* **20**: 159–186. doi:10.1175/1520-0426(2003)020<0159:AUGFVT>2.0.CO;2
- Dayton, A. I., M. T. Auer, and J. F. Atkinson. 2014. *Cladophora*, mass transport, and the nearshore phosphorus shunt. *J. Great Lakes Res.* **40**: 790–799. doi:10.1016/j.jglr.2014.05.010
- Di Toro, D. M. 1978. Optics of turbid estuarine waters: Approximations and applications. *Water Res.* **12**: 1059–1068. doi:10.1016/0043-1354(78)90051-9
- Djuricich, P., and J. Janssen. 2001. Impact of round goby predation on zebra mussel size distribution at Calumet Harbor, Lake Michigan. *J. Great Lakes Res.* **27**: 312–318. doi:10.1016/S0380-1330(01)70646-6
- Dolan, D. M., and S. C. Chapra. 2011. Great Lakes total phosphorus models and loads: A fifteen year update, final report grant no. GL 00E58501, p. 16. USEPA Great Lakes National Program Office.
- Dolan, D. M., and S. C. Chapra. 2012. Great Lakes total phosphorus revisited: 1. Loading analysis and update

- (1994–2008). *J. Great Lakes Res.* **38**: 730–740. doi:[10.1016/j.jglr.2012.10.001](https://doi.org/10.1016/j.jglr.2012.10.001)
- Fahnenstiel, G. L., and D. Scavia. 1987. Dynamics of Lake Michigan phytoplankton: Recent changes in surface and deep communities. *Can. J. Fish. Aquat. Sci.* **44**: 509–514. doi:[10.1139/f87-063](https://doi.org/10.1139/f87-063)
- Fahnenstiel, G. L., J. F. Chandler, H. J. Carrick, and D. Scavia. 1989. Photosynthetic characteristics of phytoplankton communities in Lakes Huron and Michigan: PI parameters and end-products. *J. Great Lakes Res.* **15**: 394–407. doi:[10.1016/S0380-1330\(89\)71495-7](https://doi.org/10.1016/S0380-1330(89)71495-7)
- Fahnenstiel, G. L., R. A. Stone, M. J. McCormick, C. L. Schelske, and S. E. Lohrenz. 2000. Spring isothermal mixing in the Great Lakes: Evidence of nutrient limitation and nutrient-light interactions in a suboptimal light environment. *Can. J. Fish. Aquat. Sci.* **57**: 1901–1910. doi:[10.1139/f00-144](https://doi.org/10.1139/f00-144)
- Fahnenstiel, G. L., S. Pothoven, H. Vanderploeg, D. Klarer, T. Nalepa, and D. Scavia. 2010. Recent changes in primary production and phytoplankton in the offshore region of southeastern Lake Michigan. *J. Great Lakes Res.* **36**: 20–29. doi:[10.1016/j.jglr.2010.03.009](https://doi.org/10.1016/j.jglr.2010.03.009)
- Fahnenstiel, G. L., M. J. Sayers, R. A. Shuchman, F. Yousef, and S. A. Pothoven. 2016. Lake-wide phytoplankton production and abundance in the Upper Great Lakes: 2010–2013. *J. Great Lakes Res.* **42**: 619–629. doi:[10.1016/j.jglr.2016.02.004](https://doi.org/10.1016/j.jglr.2016.02.004)
- Fairall, C., E. Bradley, D. Rogers, J. Edson, and G. Young. 1996. Bulk parameterization of air-sea fluxes for tropical ocean-global atmosphere coupled-ocean atmosphere response experiment. *J. Geophys. Res.* **101**: 3747–3764. doi:[10.1029/95JC03205](https://doi.org/10.1029/95JC03205)
- Galperin, B., L. Kantha, S. Hassid, and A. Rosati. 1988. A quasi-equilibrium turbulent energy model for geophysical flows. *J. Atmos. Sci.* **45**: 55–62. doi:[10.1175/1520-0469\(1988\)045<0055:AQETEM>2.0.CO;2](https://doi.org/10.1175/1520-0469(1988)045<0055:AQETEM>2.0.CO;2)
- Gardner, W. S., M. A. Quigley, G. L. Fahnenstiel, D. Scavia, and W. A. Frez. 1990. *Pontoporeia hoyi* – a direct link between spring diatoms and fish in Lake Michigan, p. 632–644. In M. M. Tilzer and C. Serruya [eds.], *Large lakes: Structural and functional properties*. Springer-Verlag.
- Ghedotti, M. J., J. C. Smihula, and G. R. Smith. 1995. Zebra mussel predation by round gobies in the laboratory. *J. Great Lakes Res.* **21**: 665–669. doi:[10.1016/S0380-1330\(95\)71076-0](https://doi.org/10.1016/S0380-1330(95)71076-0)
- Glyshaw, P. W., C. M. Riseng, T. F. Nalepa, and S. A. Pothoven. 2015. Temporal trends in condition and reproduction of quagga mussels (*Dreissena rostriformis bugensis*) in southern Lake Michigan. *J. Great Lakes Res.* **41**: 16–26. doi:[10.1016/j.jglr.2015.08.006](https://doi.org/10.1016/j.jglr.2015.08.006)
- Great Lakes Water Quality Protocol. 2012. Protocol amending the agreement between the United States of America and Canada on Great Lakes water quality, p. 55. International Joint Commission. Available from http://www.ijc.org/en/_/Great_Lakes_Water_Quality, accessed June, 2016.
- He, J. X., and others. 2014. Coupling age-structured stock assessment and fish bioenergetics models: A system of time-varying models for quantifying piscivory patterns during the rapid trophic shift in the main basin of Lake Huron. *Can. J. Fish. Aquat. Sci.* **72**: 7–23. doi:[10.1139/cjfas-2014-0161](https://doi.org/10.1139/cjfas-2014-0161)
- Ji, R., C. Davis, C. Chen, and R. Beardsley. 2008a. Influence of local and external processes on the annual nitrogen cycle and primary productivity on Georges Bank: A 3-D biological-physical modeling study. *J. Mar. Syst.* **73**: 31–47. doi:[10.1016/j.jmarsys.2007.08.002](https://doi.org/10.1016/j.jmarsys.2007.08.002)
- Ji, R., C. S. Davis, C. Chen, D. W. Townsend, D. G. Mountain, and R. C. Beardsley. 2008b. Modeling the influence of low-salinity water inflow on winter-spring phytoplankton dynamics in the Nova Scotian Shelf–Gulf of Maine region. *J. Plankton Res.* **30**: 1399–1416. doi:[10.1093/plankt/fbn091](https://doi.org/10.1093/plankt/fbn091)
- Johengen, T. H., H. A. Vanderploeg, and J. R. Liebig. 2013. Effects of algal composition, seston stoichiometry, and feeding rate on zebra mussel (*Dreissena polymorpha*) nutrient excretion in two Laurentian Great Lakes, p. 445–459. In T. F. Nalepa and D. W. Schloesser [eds.], *Quagga and zebra mussels: Biology, impacts and control*, 2nd ed. CRC Press.
- Kao, Y.-C., S. A. Adlerstein, and E. S. Rutherford. 2016. Assessment of top-down and bottom-up controls on the collapse of alewives (*Alosa pseudoharengus*) in Lake Huron. *Ecosystems*. **19**: 803–831. doi:[10.1007/s10021-016-9969-y](https://doi.org/10.1007/s10021-016-9969-y)
- Karatayev, A. Y., L. E. Burlakova, and D. K. Padilla. 2014. Zebra versus quagga mussels: A review of their spread, population dynamics, and ecosystem impacts. *Hydrobiologia* **746**: 1–16. doi:[10.1007/s10750-014-1901-x](https://doi.org/10.1007/s10750-014-1901-x)
- Kerfoot, W. C., J. W. Budd, S. A. Green, J. B. Cotner, B. A. Biddanda, D. J. Schwab, and H. A. Vanderploeg. 2008. Doughnut in the desert: Late-winter production pulse in southern Lake Michigan. *Limnol. Oceanogr.* **53**: 589. doi:[10.4319/lo.2008.53.2.0589](https://doi.org/10.4319/lo.2008.53.2.0589)
- Kerfoot, W. C., F. Yousef, S. A. Green, J. W. Budd, D. J. Schwab, and H. A. Vanderploeg. 2010. Approaching storm: Disappearing winter bloom in Lake Michigan. *J. Great Lakes Res.* **36**: 30–41. doi:[10.1016/j.jglr.2010.04.010](https://doi.org/10.1016/j.jglr.2010.04.010)
- Lohrenz, S. E., G. L. Fahnenstiel, D. F. Millie, O. M. E. Schofield, T. Johengen, and T. Bergmann. 2004. Spring phytoplankton photosynthesis, growth, and primary production and relationships to a recurrent coastal sediment plume and river inputs in southeastern Lake Michigan. *J. Geophys. Res.* **109**: C10S14. doi:[10.1029/2004JC002383](https://doi.org/10.1029/2004JC002383)
- Luo, L., J. Wang, D. Schwab, H. Vanderploeg, G. Leshkevich, X. Bai, H. Hu, and D. Wang. 2012. Simulating the 1998 spring bloom in Lake Michigan using a coupled physical-biological model. *J. Geophys. Res. Oceans* **117**: C10011. doi:[10.1029/2012JC008216](https://doi.org/10.1029/2012JC008216)
- Mosley, C., and H. Bootsma. 2015. Phosphorus recycling by profunda quagga mussels (*Dreissena rostriformis bugensis*) in Lake Michigan. *J. Great Lakes Res.* **41**: 38–48. doi:[10.1016/j.jglr.2015.07.007](https://doi.org/10.1016/j.jglr.2015.07.007)

- Nalepa, T. F., J. F. Cavaletto, M. Ford, W. M. Gordon, and M. Wimmer. 1993. Seasonal and annual variation in weight and biochemical content of the zebra mussel, *Dreissena polymorpha*, in Lake St. Clair. *J. Great Lakes Res.* **19**: 541–552. doi:10.1016/S0380-1330(93)71240-X
- Nalepa, T. F., D. L. Fanslow, and G. A. Lang. 2009. Transformation of the offshore benthic community in Lake Michigan: Recent shift from the native amphipod *Diporeia spp.* to the invasive mussel *Dreissena rostriformis bugensis*. *Freshw. Biol.* **54**: 466–479. doi:10.1111/j.1365-2427.2008.02123.x
- Pothoven, S. A., D. L. Fanslow, and G. L. Fahnenstiel. 2012. Lipid content of *Mysis diluviana* in the offshore region of southeastern Lake Michigan in 2009–2010. *J. Great Lakes Res.* **38**: 561–568. doi:10.1016/j.jglr.2012.05.003
- Pothoven, S. A., and G. L. Fahnenstiel. 2013. Recent change in summer chlorophyll a dynamics in southeastern Lake Michigan. *J. Great Lakes Res.* **39**: 287–294. doi:10.1016/j.jglr.2013.02.005
- Pothoven, S. A., and G. L. Fahnenstiel. 2015. Spatial and temporal trends in zooplankton assemblages along a near-shore to offshore transect in southeastern Lake Michigan from 2007 to 2012. *J. Great Lakes Res.* **41**: 95–103. doi:10.1016/j.jglr.2014.09.015
- Rowe, M. D., E. J. Anderson, J. Wang, and H. A. Vanderploeg. 2015a. Modeling the effect of invasive quagga mussels on the spring phytoplankton bloom in Lake Michigan. *J. Great Lakes Res.* **41**: 49–65. doi:10.1016/j.jglr.2014.12.018
- Rowe, M. D., D. R. Obenour, T. F. Nalepa, H. A. Vanderploeg, F. Yousef, and W. C. Kerfoot. 2015b. Mapping the spatial distribution of the biomass and filter-feeding effect of invasive dreissenid mussels on the winter-spring phytoplankton bloom in Lake Michigan. *Freshw. Biol.* **60**: 2270–2285. doi:10.1111/fwb.12653
- Saulquin, B., A. Hamdi, F. Gohin, J. Populus, A. Mangin, and O. F. d'Andon. 2013. Estimation of the diffuse attenuation coefficient K_{dPAR} using MERIS and application to seabed habitat mapping. *Remote Sens. Environ.* **128**: 224–233. doi:10.1016/j.rse.2012.10.002
- Scavia, D., G. A. Lang, and J. F. Kitchell. 1988. Dynamics of Lake Michigan plankton: A model evaluation of nutrient loading, competition, and predation. *Can. J. Fish. Aquat. Sci.* **45**: 165–177. doi:10.1139/f88-018
- Schneider, D. W. 1992. A bioenergetics model of zebra mussel, *Dreissena polymorpha*, growth in the Great Lakes. *Can. J. Fish. Aquat. Sci.* **49**: 1406–491416. doi:10.1016/j.jglr.2014.12.018
- Schwab, D. J., and D. Beletsky. 1998. Lake Michigan mass balance study: Hydrodynamic modeling project, p. 53. ERL GLERL-108, NOAA GLERL.
- Steele, J. H., and E. W. Henderson. 1992. The role of predation in plankton models. *J. Plankton Res.* **14**: 157–172. doi:10.1093/plankt/14.1.157
- Sverdrup, H. U. 1953. On conditions for the vernal blooming of phytoplankton. *J. Cons. Perm. Int. Explor. Mer.* **18**: 287–295.
- Tian, R., and C. Chen. 2006. Influence of model geometrical fitting and turbulence parameterization on phytoplankton simulation in the Gulf of Maine. *Deep-Sea Res. Part II Top. Stud. Oceanogr.* **53**: 2808–2832. doi:10.1016/j.dsr2.2006.08.006
- Tian, R. C. 2006. Toward standard parameterizations in marine biological modeling. *Ecol. Model.* **193**: 363–386. doi:10.1016/j.ecolmodel.2005.09.003
- Troy, C. D., S. Ahmed, N. Hawley, and A. Goodwell. 2012. Cross-shelf thermal variability in southern Lake Michigan during the stratified periods. *J. Geophys. Res. Oceans* **117**: C02028. doi:10.1029/2011JC007148
- Turschak, B. A., D. Bunnell, S. Czesny, T. O. Höök, J. Janssen, D. Warner, and H. A. Bootsma. 2014. Nearshore energy subsidies support Lake Michigan fishes and invertebrates following major changes in food web structure. *Ecology* **95**: 1243–1252. doi:10.1890/13-0329.1
- Vanderploeg, H., and others. 2012. Seasonal zooplankton dynamics in Lake Michigan: Disentangling impacts of resource limitation, ecosystem engineering, and predation during a critical ecosystem transition. *J. Great Lakes Res.* **38**: 336–352. doi:10.1016/j.jglr.2012.02.005
- Vanderploeg, H. A. 1994. Zooplankton particle selection and feeding mechanisms, p. 205–234. *In* R. S. Wotton [ed.], *The Biology of Particles in Aquatic Systems*. Lewis Publishers, Ann Arbor, Michigan.
- Vanderploeg, H. A., W. S. Gardner, C. C. Parrish, J. R. Liebig, and J. F. Cavaletto. 1992. Lipids and life-cycle strategy of a hypolimnetic copepod in Lake Michigan. *Limnol. Oceanogr.* **37**: 413–424. doi:10.4319/lo.1992.37.2.0413
- Vanderploeg, H. A., and others. 2009. Hypoxia affects spatial distributions and overlap of pelagic fish, zooplankton, and phytoplankton in Lake Erie. *J. Exp. Mar. Biol. Ecol.* **381**: S92–S107. doi:10.1016/j.jembe.2009.07.027
- Vanderploeg, H. A., J. R. Liebig, T. F. Nalepa, G. L. Fahnenstiel, and S. A. Pothoven. 2010. *Dreissena* and the disappearance of the spring phytoplankton bloom in Lake Michigan. *J. Great Lakes Res.* **36**: 50–59. doi:10.1016/j.jglr.2010.04.005
- Vanderploeg, H. A., and others. 2015. Spatial and predatory interactions of visually preying nonindigenous zooplankton and fish in Lake Michigan during midsummer. *J. Great Lakes Res.* **41**: 125–142. doi:10.1016/j.jglr.2015.10.005
- Wang, J., X. Bai, H. Hu, A. Clites, M. Colton, and B. Lofgren. 2012. Temporal and spatial variability of Great Lakes ice cover, 1973–2010. *J. Clim.* **25**: 1318–1329. doi:10.1175/2011JCLI4066.1
- Warner, D. M., and B. M. Lesht. 2015. Relative importance of phosphorus, invasive mussels and climate for patterns in chlorophyll a and primary production in Lakes Michigan and Huron. *Freshw. Biol.* **60**: 1029–1043. doi:10.1111/fwb.12569
- Yousef, F., W. C. Kerfoot, R. Shuchman, and G. Fahnenstiel. 2014. Bio-optical properties and primary production of Lake Michigan: Insights from 13-years of SeaWiFS

imagery. J. Great Lakes Res. **40**: 317–324. doi:[10.1016/j.jglr.2014.02.018](https://doi.org/10.1016/j.jglr.2014.02.018)

Limnology and Ecosystems Research (CILER) through the NOAA Cooperative Agreement with the University of Michigan (NA12OAR4320071).

Acknowledgments

FVCOM and GEM codes are available at <http://fvcom.smast.umassd.edu/>. Nancy Morehead conducted phosphorus analysis on mussel tissue. David Dolan provided nutrient loading data, and preliminary analysis by M. D. Rowe was supported by the US EPA research associate program at the Large Lakes Research Station. This is CILER contribution number 1112 and GLERL contribution number 1855. M. D. Rowe received funding from the National Research Council Research Associate program and Cooperative Institute for

Conflict of Interest

None declared.

Submitted 30 August 2016

Revised 13 February 2017; 14 April 2017

Accepted 18 April 2017

Associate editor: Yong Liu